5'-cap RNA/SAM mimetic conjugates as bisubstrate inhibitors of viral RNA cap 2'-O-methyltransferases

Rostom Ahmed-belkacem, Priscila Sutto-Ortiz, Adrien Delpal, Joris Troussier, Bruno Canard, Jean-Jacques Vasseur, Etienne Decroly, Françoise Debart

5’-cap RNA/SAM mimetic conjugates as bisubstrate inhibitors of viral RNA cap 2'-*O*-methyltransferases

Rostom Ahmed-Belkacem,[1] Priscila Sutto-Ortiz,[2] Adrien Delpal,[2] Joris Troussier,[1] Bruno Canard,[2] Jean-Jacques Vasseur,[1] Etienne Decroly,[2,*] and Françoise Debart[1,*]

[1]IBMM, University of Montpellier, CNRS, ENSCM, Montpellier, France
[2]AFMB, University of Aix-Marseille, CNRS, Marseille, France

*corresponding authors
francoise.debart@umontpellier.fr; etienne.decroly@univ-amu.fr

full postal address: [1]IBMM, Pôle Chimie Balard Recherche, 1919 route de Mende, 34293 Montpellier cedex 5, France

ABSTRACT

Viral RNA cap 2’-*O*-methyltransferases are considered promising therapeutic targets for antiviral treatments, as they play a key role in the formation of viral RNA cap-1 structures to escape the host immune system. A better understanding of how they interact with their natural substrates (RNA and the methyl donor SAM) would enable the rational development of potent inhibitors. However, as few structures of 2’-*O*-MTases in complex with RNA have been described, little is known about substrate recognition by these MTases. For this, chemical tools mimicking the state in which the cap RNA substrate and SAM cofactor are bound in the enzyme’s catalytic pocket may prove useful. In this work, we designed and synthesized over 30 RNA conjugates that contain a short oligoribonucleotide (ORN with 4 or 6 nucleotides) with the first nucleotide 2’-*O*-attached to an adenosine by linkers of different lengths and containing *S* or *N*-heteroatoms, or a 1,2,3-triazole ring. These ORN conjugates bearing or not a cap structure at 5’-extremity mimic the methylation transition state with RNA substrate/SAM complex as bisubstrates of 2’-*O*-MTases. The ORN conjugates were synthesized either by the incorporation of a dinucleoside phosphoramidite during RNA elongation or by click chemistry performed on solid-phase post-RNA elongation. Their ability to inhibit the activity of the nsp16/nsp10 complex of SARS-CoV-2 and the NS5 protein of dengue and Zika viruses was assessed. Significant submicromolar IC_{50} values and K_d values in the µM range were found, suggesting a possible interaction of some ORN conjugates with these viral 2’-*O*-MTases.

Keywords (10 max)

Cap RNA; SAM analogues; conjugate; bisubstrate; inhibitor; dengue virus; SARS-CoV-2; 2’-*O*-methyltransferase; NS5 protein; nsp16 protein.

1. Introduction

In eukaryotes and RNA viruses, RNA methylation is one of the most important post-transcriptional modifications of RNA, which is attracting growing interest in the field of epitranscriptomics, as it plays a crucial role in RNA stability, splicing, translation and as self-marker [1]. The methylation reaction is catalyzed by RNA methyltransferases (MTases) that use *S*-adenosyl-L-methionine (SAM) as a cofactor to transfer the methyl group to the 5'-terminal RNA cap or, internally, along the RNA sequence, releasing *S*-adenosyl-L-homocysteine (SAH). Methylation of ribonucleotides occurs at various positions on the nucleobase (^{7m}G, m^{6}A, m^{5}C, m^{1}A…) or ribose moieties [2, 3]. In particular, the methylation of the 2'-hydroxyl of the nucleotide ribose (N_m) is a ubiquitous epitranscriptomic modification often introduced at the first and second transcribed nucleotides downstream of the ^{7m}G cap by 2'-*O*-methyltransferases (2'-*O*-MTases) giving rise to cap-1 (^{7m}GpppN$_m$) or cap-2 (^{7m}GpppN$_m$N$_m$) [4]. 2'-*O*-methyl nucleotides have also been observed at internal sites of many RNA species, yet we have focused on 2'-*O*-methylation of the viral mRNA cap. This methyl decoration is important for RNA viruses to evade host innate immune responses by preventing recognition of their mRNAs as "non-self" by RIG like receptors as RIG-I and MDA5 [5-7]. Viral 2'-*O*-MTases therefore represent potential targets for antiviral drug development and for investigating unidentified molecular mechanisms of cap-1/2 formation, which underlies innate immunity evasion by viruses [8, 9]. It is noteworthy that even though most of 2'-*O*-MTases share a common Rossmann fold structural organization, the mechanism governing RNA recognition and their enzymatic activities varies among RNA viruses. For instance, in Flaviviruses (such as dengue (DENV) and Zika viruses (ZIKV)), the NS5 protein carries both *N*7- and 2'-*O*-MTase activities [10-13]. In contrast, coronaviruses encode two distinct enzymes: an *N*7-MTase in the C-terminal domain of nsp14 and a 2'-*O*-MTase on nsp16, which is regulated by a cofactor nsp10 [14-16]. A better understanding of how these proteins interact with their natural substrate and co-factor (mRNA and SAM) would enable to better know the environment of these MTases and design more potent inhibitors. Although several MTases have already been crystallized with or without the presence of a ligand (SAM, SAH, inhibitor) [17-19] or with cap analogs [11, 20], but to our knowledge only a limited set of MTases have been crystallized as ternary complexes with mRNA and SAM or SAH [21-24]. In some of these structures, the viral genome is outside the basic putative RNA binding groove, suggesting that the structure may represent a snapshot of the guanylylation reaction of the viral genome prior to its repositioning to reach the methyl donor sites [22]. Based on the results reported on RlmJ, a bacterial m^{6}A rRNA MTase [25], we suggest that by designing short RNA covalently linked to a SAM analogue through the 2'-position of the 5'-terminal nucleotide (2'-*O*-methylation site), the interaction of the SAM mimetic with the protein could stabilize the RNA in the MTase methylation site, enabling its co-crystallization or its inhibition.

In a search for inhibitors of viral 2'-*O*-MTases and in contrast to existing small molecule inhibitors described for these targets [26-30], we chose to explore the promising bisubstrate approach with more complex molecules as a selective method of targeting MTases [31]. The bisubstrate molecules are designed as a representation of the transition state reached during the methylation reaction catalyzed by the MTase in the presence of the SAM methyl donor and the substrate [32]. Therefore, most RNA MTase bisubstrates consist of a SAM analogue linked to a molecule mimicking the RNA substrate. Recently, this approach has been used to target m^6A MTases, valuable enzymes involved in a common post-transcriptional RNA modification with complex regulatory mechanisms [25, 33-36]. In these studies, a SAM analogue is connected *via* different linkers to the *N*6-atom of an adenosine within dinucleo(s)tides, a trinucleotide or a 13-mer RNA. As for our work, a similar bisubstrate approach was used to mimic the transition state of 2'-*O*-methylation of mRNA, with the design of dinucleosides with a 5'-OH adenosine in place of the first nucleotide downstream of the RNA cap (A1) linked from its 2' position to the 5' position of a second adenosine in place of the SAM adenosine (A2), *via* linkers of different sizes containing various heteroatoms (S, N) [31, 37]. Surprisingly, none of the synthesized 2',5'-linked dinucleosides showed inhibition of viral and human RNA 2'-*O*-MTases and, against all expectations, some displayed selective inhibition of nsp14, the *N*7-MTase of SARS-CoV [37]. The most plausible explanation for the lack of 2'-*O*-MTases inhibition of these dinucleosides is the absence of a cap structure which plays a key role for RNA recognition by RNA 2' *O*-MTases. Indeed, the presence of a cap binding pocket allows the stacking of the GTP moieties by a phenylalanine residue (F25) in the NS5 2'-*O*-MTase of Zika or dengue flaviviruses [38, 39] and contributes to the ability of these MTases to recognize with high affinity 5'-cap mRNA (Gppp-mRNA) [10, 40], or specifically 5'-cap-0 mRNAs (^{7m}Gppp-mRNA) as illustrated by nsp16 2'-*O*-MTase of SARS-CoV and SARS-CoV-2 [17, 24, 41].

We then hypothesized that short 5'-cap RNA structure inserting these 2',5'-linked dinucleosides might be good substrates for viral 2'-*O*-MTases, particularly those of dengue/Zika viruses and SARS-CoVs. To test this assumption, we report here the chemical synthesis on an automated DNA/RNA synthesizer of over 30 short oligoribonucleotides (ORNs) carrying various dinucleosides (X) in place of the 5'-terminal nucleotide of the RNA downstream of the cap. The sequences of the ORN-X conjugates prepared are composed of the first nucleotides of the viral RNA sequence of dengue/Zika viruses (5'-AGUUGU) [42], SARS-CoV (5'-AUAUUA) [43] or SARS-CoV-2 (5'-AUUAAA) [44]. In ORN-X conjugates, the first nucleotide downstream of the cap, which is naturally an adenosine, has been replaced by an adenine dinucleoside (X). Three series of capped or uncapped ORN-X of 4 or 6 nucleotides were prepared with at their 5'-end, different dinucleosides bearing a *S*-methylthioether linker (S-series, X^S), *N*-ethylamino (X^N) and *N*-ethyl-*N*-nosyl-amino (N^{NS}) linkers (N-series) or a methyltriazole linker (Tz-series, X^{Tz}) between the two adenosines A_1 and A_2 (Fig. 1). Some of the ORN-X synthesized were evaluated *in vitro* as potential

inhibitors of the 2'-*O*-MTase activity of NS5 proteins from dengue and Zika viruses and the nsp16/nsp10 protein complex from SARS-CoV-2. Remarkably, IC_{50} values in the sub-µM range, suggesting a possible interaction of certain ORN conjugates with these viral 2'-*O*-MTases were confirmed by K_d values in the µM range with NS5 from dengue virus.

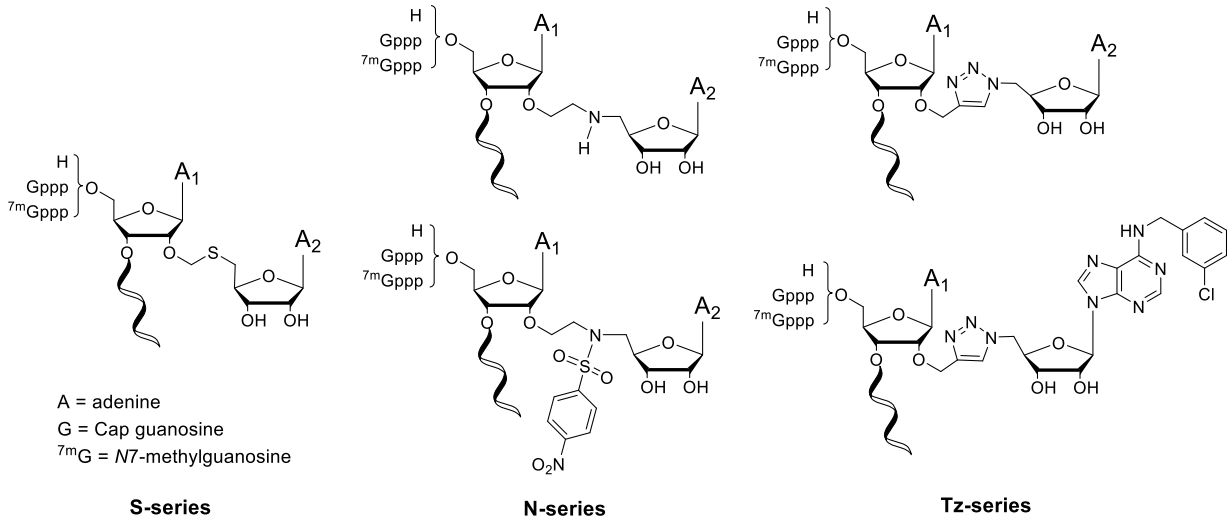

Figure 1. Schematic representation of ORN-X containing adenine dinucleosides (X) bearing *S*-methylthioether linker (ORN-X^S) (S-series), *N*-ethylamino (ORN-X^N) and *N*-ethyl-*N*-nosyl-amino linkers (ORN-X^{Ns}) (N-series) or a methyltriazole linker (ORN-X^{Tz}) (Tz-series)

2. Results and discussion

To synthesize ORN-X conjugates, two strategies were used for linker formation within dinucleosides X. Both *S*- and *N*-containing linkers between the two adenosines A_1 and A_2 were formed prior to ORN elongation on a solid support, by first preparing the corresponding 3'-phosphoramidite dinucleosides X^S **1** and X^{Ns} **2** (Schemes 1 and 2). Dinucleosides **1** and **2** were then incorporated into the 5'-end of the ORN chain, and the capping reaction was performed on solid-phase prior to deprotection of the ORN-X and its release from the support. Another strategy was used for the triazole-containing linker formed on a solid support, under copper-catalyzed azide–alkyne cycloaddition (CuAAC) conditions following ORN chain elongation and capping processes.

2.1. Synthesis of ORN-X *via* dinucleoside phosphoramidite incorporation (for S-series and N-series)

*2.1.1. Synthesis of dinucleoside phosphoramidites X^S **1** and X^{Ns} **2***

The 3'-*O*-(2-cyanoethyl-*N,N*-diisopropylphosphoramidite)phosphoramidite **1** of the adenine dinucleoside 2',5'-bridged by a sulfur-containing linker was obtained in 5 steps from the previously

described S-dinucleoside **3** protected by a 5',3'-*O*-*tetra*isopropyldisiloxane group on A_1 (Schema 1) [31]. First, compound **3** was subjected to selective 2',3'-*O*-acetylation with acetic anhydride at 0°C to give **4** in 98% yield [45]. The reaction at 0°C prevents acetylation of the nucleobases. Next, the exocyclic *N*6 amino functions of adenines were protected by a phenoxyacetyl (Pac) group with Pac anhydride at 25°C in pyridine/THF [46]. We noted here that no reaction occurred in pyridine alone. Resulting compound **5** obtained in 78% yield was desilylated with a fluoride treatment to afford dinucleoside **6** with 5',3'-OH in A_1 (80% yield) [47]. A dimethoxytrityl group was then introduced onto the 5'-OH in 94% yield. The reaction was performed at 60°C as attempts at room temperature and even at 40°C failed. Finally, the resulting dinucleoside **7** was subjected to phosphitylation with 2-cyanoethyl *N,N'*-diisopropylchlorophosphoramidite to give rise to the desired dinucleoside phosphoramidite **1** in 43% yield contaminated with its oxidation product **8** in a 50/50 mixture as determined by ^{31}P-NMR [48]. As phosphoramidate **8** is not reactive during the coupling step of ORN elongation on solid support, the mixture of **1** and **8** was used as is for ORN-X^S synthesis.

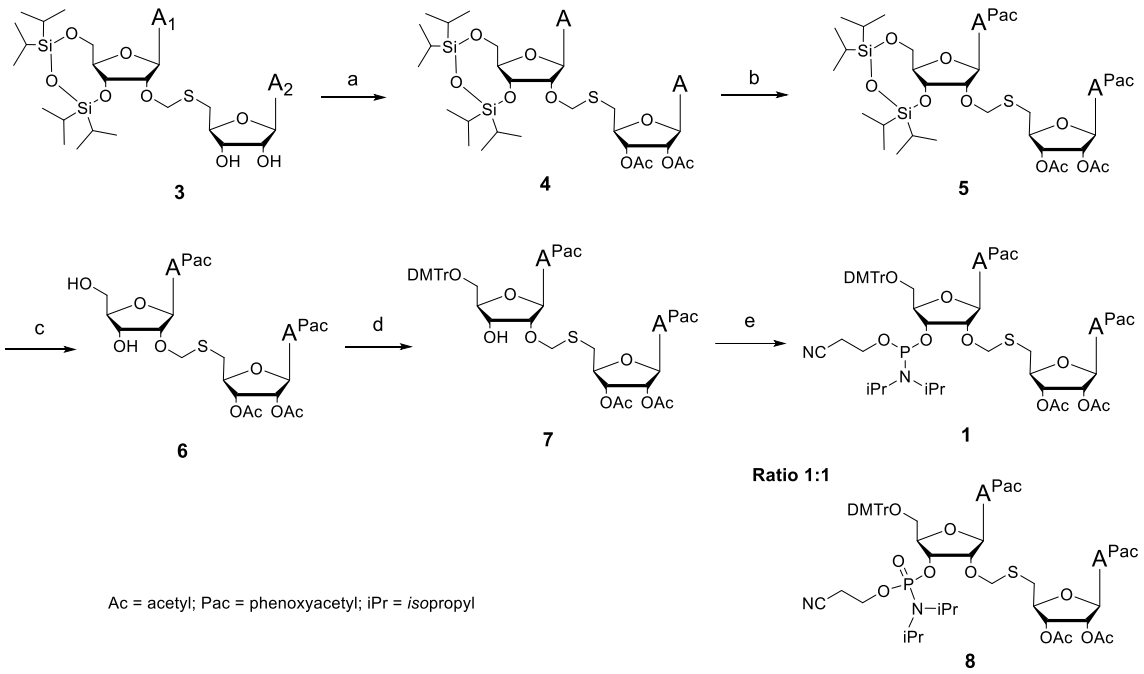

Scheme 1. Synthesis of dinucleoside phosphoramidite X^S **1**.

Reagents and conditions : (a) Ac_2O, pyridine, 0 °C, 3 h, 98%; (b) Pac_2O, pyridine/THF, 25°C, 15 h, 74%; (c) $Et_3N.3HF$, THF, 40°C, 17 h, 80%; (d) DMTrCl, pyridine, 60°C, 4 h, 94%; (e) 2-cyanoethyl *N*,*N*-di*iso*propylchlorophosphoramidite, DIEA, DCM, 25°C, 80 min, 43%.

The dinucleoside 3'-*O*-phosphoramidite **2** with an ethylamino linker between the two adenosines was prepared from the previously described 5',3'-di-*O*-TBS-2'-*O*-(tosylethyl) adenosine **9** [31] and from 5'-*O*-tosyl-2,3'-di-*O*-acetyl adenosine **10** obtained in 80% yield from 5'-*O*-tosyl adenosine **11** by reaction with acetic anhydride (Scheme 2). Reaction in basic medium between **9** and 4-nitrobenzenesulfonamide led to protection of the 2'-*O*-ethylamino substituent of nucleoside **12** by a

nosyl group in 74% yield [49]. Basic nucleophilic substitution of tosylate **10** by sulfonamide **12** creates the *N*-nosyl ethylamino internucleoside bond between A_1 and A_2 of **13** in 56% yield. As with phosphoramidite **1**, the exocyclic amino functions of the adenines of **13** were protected by phenoxyacetyl (Pac) groups in pyridine/THF to give **14** (76% yield), then the silyl protections were removed from A_1 to afford 5',3'-OH dinucleoside **15** (81% yield). DMTr protection was added at 60°C to the 5'-OH of **15** to give **16** (88% yield), which was then 3'-*O*-phosphitylated leading to phosphoramidite **2** (56% yield).

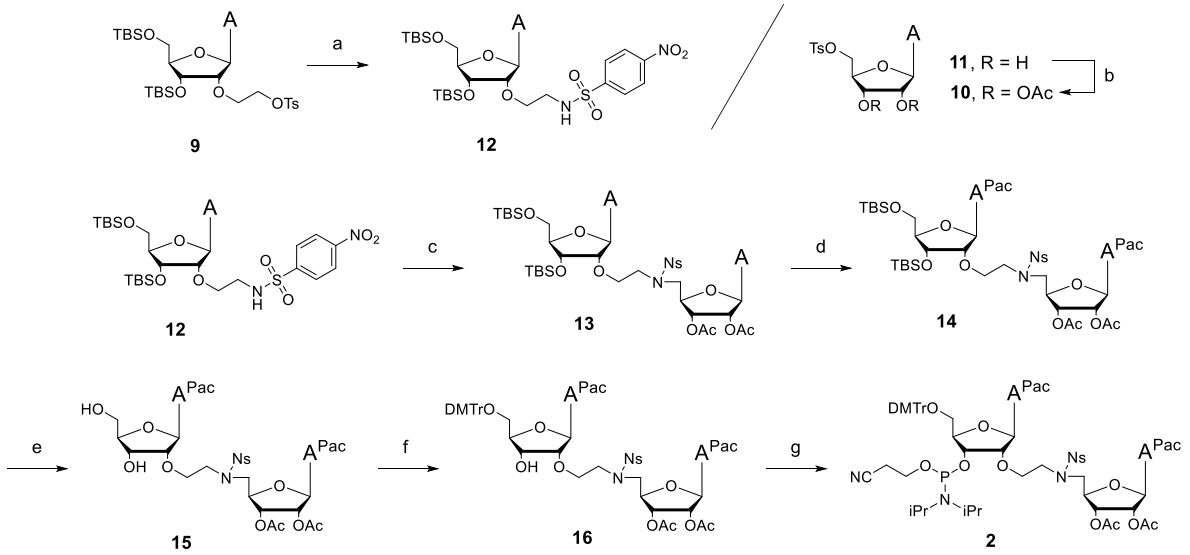

Scheme 2. Synthesis of dinucleoside phosphoramidite X^{Ns} **2**.

Reagents and conditions: (a) 4-nitrobenzenesulfonamide, KI, K_2CO_3, DMF, 50°C, 24 h, 74%; (b) Ac_2O, pyridine, 0°C, 3 h, 80%; (c) **10**, KI, K_2CO_3, DMF, 50°C, 24 h, 56%; (d) Pac_2O, pyridine/THF, 25°C, 24 h, 76%; (e) $Et_3N.3HF$, THF, 40°C, 24 h, 81%; (f) DMTrCl, pyridine, 60°C, 4 h, 88%; (g) 2-cyanoethyl *N,N*-di*iso*propylchlorophosphoramidite, DIEA, DCM, 25°C, 90 min, 56%.

2.1.2. Synthesis of ORN-X^S and ORN-X^{Ns} conjugates

Dinucleoside phosphoramidites **1** and **2** were incorporated into 4-mer and 6-mer oligoribonucleotides using the same coupling conditions (180 s) as for the other ribonucleoside phosphoramidites, according to the 1 µmole solid-support oligoribonucleotide synthesis described by us [50]. The 5'-OH ORN-X and Gppp-ORN-X of the S- and N-series were synthesized using A, G and U ribonucleoside phosphoramidites protected by 2'-*O*-pivaloyloxymethyl (PivOM) groups (from Chemgenes, USA)) (Schemes 3 and 4) [50]. To obtain ^{7m}GpppORN-X, the PivOM phosphoramidite synthons were replaced by 2'-*O*-propionyloxymethyl (PrOM) ribonucleoside phosphoramidites, which allow the use of milder basic deprotection conditions to preserve cap-0 integrity as we recently reported [51].

As **1** was contaminated with phosphoramidate compound **8**, the coupling step was repeated twice before regular oxidation. 5'-OH ORN-X with adenine dinucleosides containing the methylthio X^S or the

N-nosyl ethylamino X^{Ns} linker were then deprotected and cleaved from the solid support using two-step deprotection under basic conditions, i.e. DBU followed by aqueous ammonia at room temperature, conditions described for RNA synthesis following the PivOM strategy [50]. To obtain 5'-OH ORN containing the *N*-ethylamino adenine dinucleoside X^N, additional treatment with thiophenol and DBU was applied to remove the nosyl group prior to basic treatment. Crude ORN-X were purified by ion-exchange HPLC, and pure ORN-X^S, ORN-X^N and ORN-X^{Ns} conjugates were characterized by MALDI-TOF mass spectrometry. Note that MALDI-TOF analysis of ORN-X^{Ns} shows, alongside the expected ion, lower mass ions corresponding to ions resulting from known mono- and di-photo deoxygenations of the nitro group occurring during the laser irradiation of the samples (see supplementary material) [52].

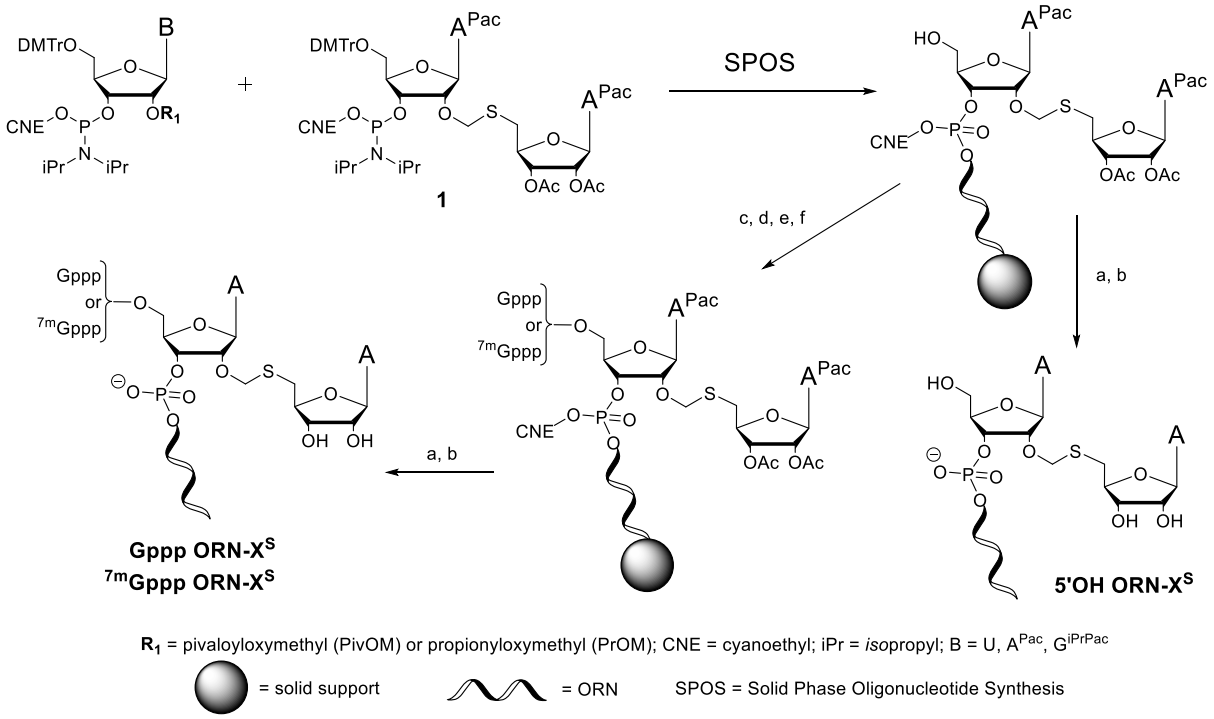

Scheme 3. On-column synthesis of 5'-OH ORN-X^S, GpppORN-X^S and ^{7m}GpppORN-X^S conjugates with dinucleoside X^S as a 5'-terminal nucleotide analogue.

Reagents and conditions : (a) 1M DBU / MeCN, 25°C, 3 min; (b) for OH or GpppORN-X^S: aq. NH_3 40°C, 3 h; for ^{7m}GpppORN-X^S: 7M NH_3 in MeOH, 40°C, 3 h; (c) diphenylphosphite / pyridine, 40°C, 35 min; (d) 0.1 M TEAB, pH 8, 40°C, 45 min; (e) imidazole, $CBrCl_3$, BSA, Et_3N, MeCN, 40°C, 1 h; (f) for GpppORN-X^S: 5'-diphosphate guanosine tri-*n*-butylammonium salt, $ZnCl_2$ / DMF, 40°C, 18 h; for ^{7m}GpppORN-X^S: 5'-diphosphate *N*7-methylguanosine tri-*n*-butylammonium salt, $ZnCl_2$ / DMF, 40°C, 18 h.

5'-Cap GpppORN-X and 5'-Cap-0 ^{7m}GpppORN-X were obtained using our overall chemical process previously described [51, 53]. The introduction of unmethylated and *N*7-methylated caps onto ORN-X was performed on solid support at the end of ORN elongation (Schemes 3 and 4). As *N*7-methylguanosine is unstable in basic media during ORN deprotection, the 2'-*O*-PivOM protecting

groups were replaced by more base-labile 2'-*O*-PrOM groups, and standard aqueous ammonia was replaced by 7M methanolic ammonia to release the ORN-X [51]. As with the preparation of 5'-OH ORN-X^N, the capped ORN-X^N required additional thiophenolate treatment upon deprotection of the capped ORN-X^{Ns} (Scheme 4). Finally, GpppORN-X were deprotected and cleaved from the solid support with DBU followed by aqueous ammonia treatment, while methanolic ammonia was used to yield ^{7m}GpppORN-X.

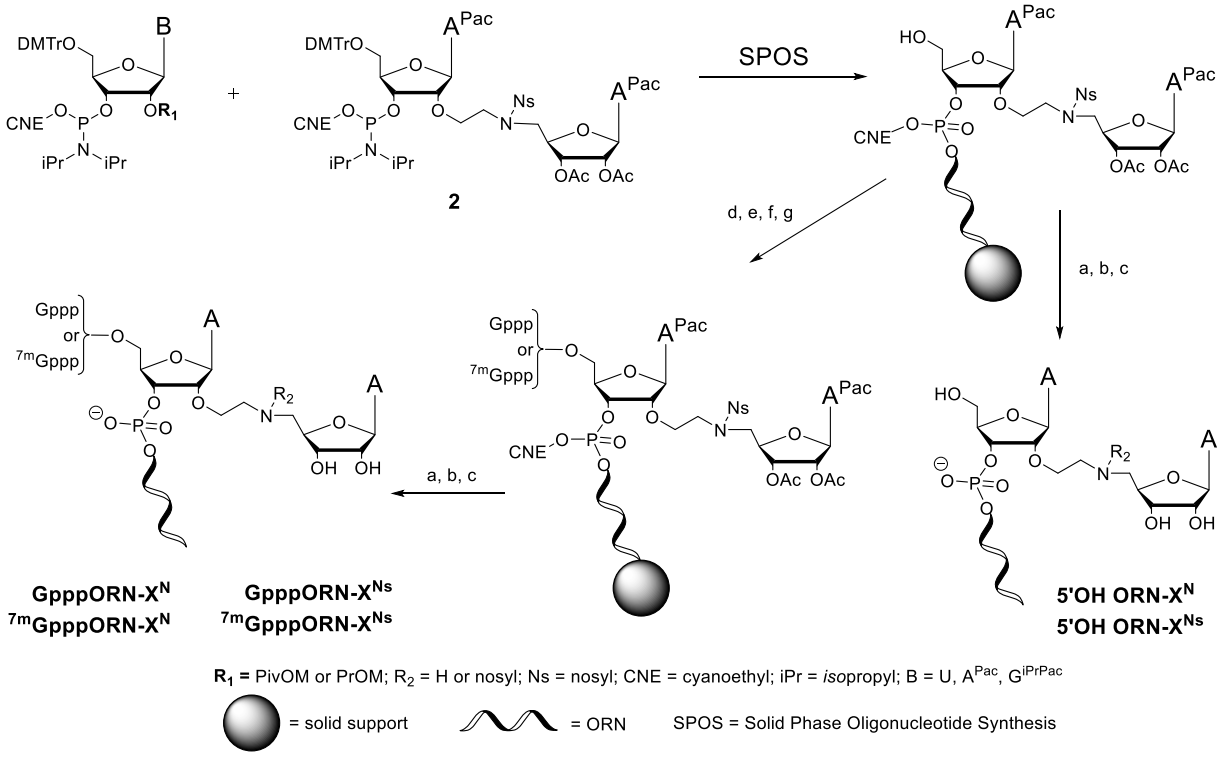

Scheme 4. On-column synthesis of 5'OH ORN-X, GpppORN-X and ^{7m}GpppORN-X conjugates of the N-series with dinucleosides X^{Ns} and X^N as 5'-terminal nucleotide analogues.

Reagents and conditions : (a) only for ORN containing X^N: PhSH / DBU /DMF, 40°C, 18 h; (b) 1M DBU / MeCN 25°C, 3 min; (c) for OH or GpppORN-X: aq. NH_3 40°C, 3 h; for ^{7m}GpppORN-X: 7M NH_3 / MeOH; (d) diphenylphosphite / pyridine, 40°C, 35 min; (e) 0.1M TEAB, pH 8, 40°C, 45 min; (f) imidazole, $CBrCl_3$, BSA, Et_3N, MeCN, 40°C, 1 h; (g) for GpppORN-X: 5'-diphosphate guanosine tri-*n*-butylammonium salt, $ZnCl_2$ / DMF, 40°C, 18 h; for ^{7m}GpppORN-X: 5'-diphosphate *N*7-methylguanosine tri-*n*-butylammonium salt, $ZnCl_2$ / DMF, 40°C, 18 h.

2.2. Synthesis of ORN-X^{TZ} conjugates with a methyltriazole linker

In the case of the Tz-series ORN, a different strategy was used to create the internucleoside linker between A_1 and A_2 (Scheme 5). Instead of preparing a dinucleoside with the methyltriazole linker and then introducing it into the ORN, the linker was formed at the end of ORN elongation on a solid support by CuAAC. A propargyl function was introduced into ORN *via* the use of the commercially available adenosine 2'-*O*-propargyl-3'-*O*-phosphoramidite **17**. CuAAC between the 2'-*O*-propargyl function of adenosine A_1 in ORN and 5'-azido adenosine **18** or its adenine analogue **19** was carried out in the

presence of copper (II) and sodium ascorbate under microwave irradiation (Scheme 5) [54, 55]. Click chemistry was performed on the capped ORN on solid support and, as reported in the literature, the cap structure, particularly the ^{7m}G motif remained stable under these conditions [56, 57]. Note that Ethève-Quelquejeu et al. have used a similar linker to connect the *N*6 or *N*1 position of an adenine bearing a propargyl group to the 5'position of another adenosine as a SAM mimic in order to obtain bisubstrate interfering with m^6A and m^1A RNA MTases [35, 36].

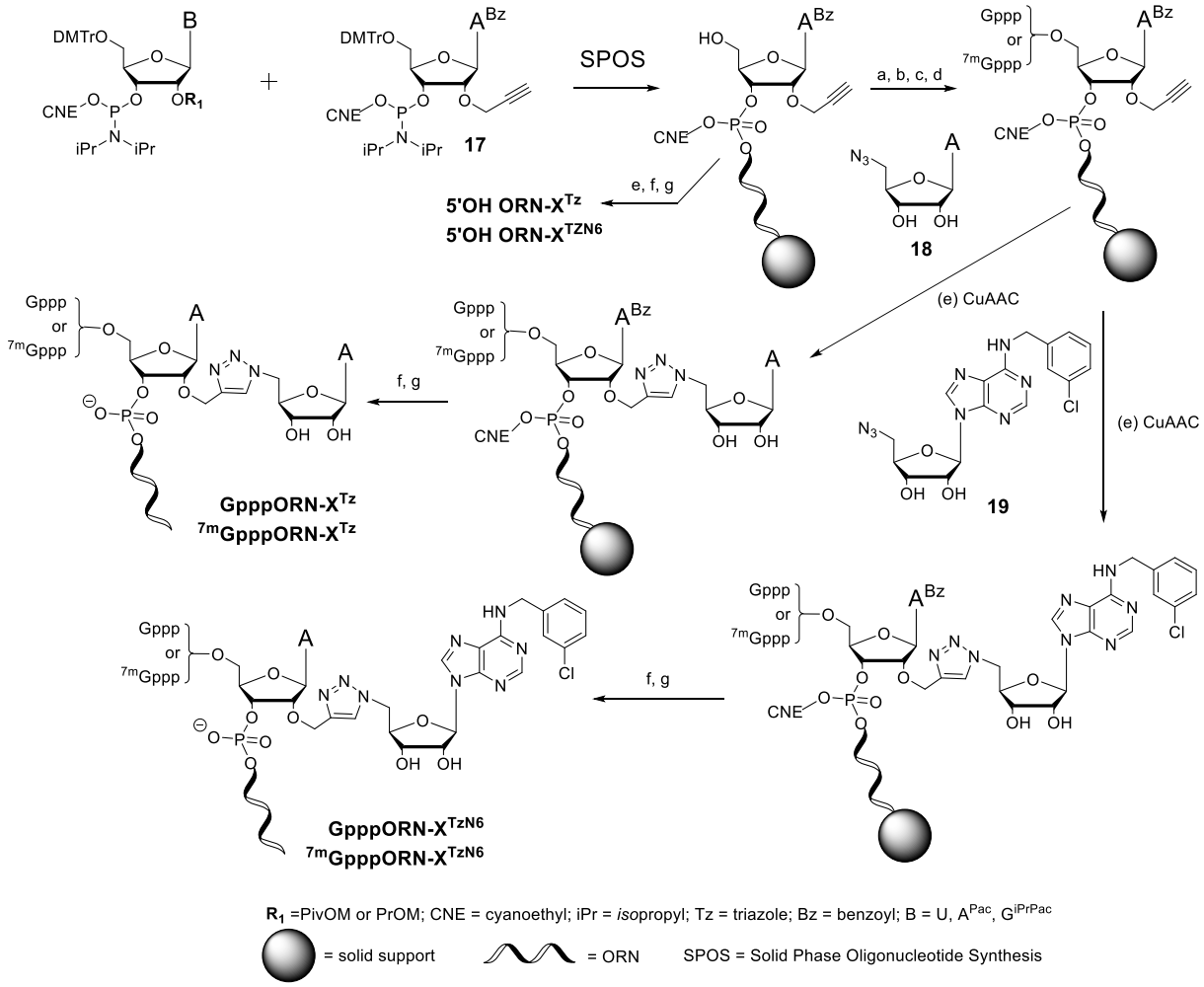

Schema 5. Synthesis of 5'OH ORN-X^{Tz}, GpppORN-X^{Tz} and ^{7m}GpppORN-X^{Tz} conjugates with dinucleosides X^{Tz} and X^{TzN6} containing *N*6-*meta*-chlorobenzyl adenosine, as 5'-terminal nucleotide analogues.

Reagents and conditions : ; (a) diphenylphosphite / pyridine, 40°C, 35 min; (b) 0.1M TEAB, pH 8, 40°C, 45 min; (c) imidazole, $CBrCl_3$, BSA, Et_3N, MeCN, 40°C, 1 h; (d) for GpppORN: 5'-diphosphate guanosine tri-*n*-butylammonium salt, $ZnCl_2$ / DMF, 40°C, 18 h; for ^{7m}GpppORN: 5'-diphosphate *N*7-methylguanosine tri-*n*-butylammonium salt, $ZnCl_2$ / DMF, 40°C, 18 h; (e) **18** or **19**, $CuSO_4$, sodium ascorbate, dioxane/H_2O, 65°C MW, 1 h; (f) 1M DBU / MeCN, 25°C, 3 min; (g) for 5'OH ORN-X or GpppORN-X: aq.NH_3, 40°C, 3 h; for ^{7m}GpppORN-X: 7M NH_3 / MeOH.

For the ORN-X^{Tz} synthesis, 5'-Azido adenosine **18** was obtained from 2',3'-*O*-isopropylidene adenosine in two steps (Scheme S1). In the first step, the azido function was introduced in the presence of

diphenylphosphoryl azide (DPPA) followed by treatment with sodium azide, giving rise to nucleoside **20** [58]. Next, isopropylidene was removed in acidic medium to afford **18**.

Flavivirus NS5 proteins have a unique conserved cavity, known to accommodate RNA cap structure (by stacking interaction mediated by F25) close to the SAM binding site [59]. Benzyl groups, in particular the *meta*-chlorobenzyl substituent on the N6 exocyclic amine of SAH adenine, have been shown to accommodate this cavity and provide inhibitors with enhanced activity and selectivity towards dengue 2'-*O*-MTase [26]. In a similar way, the exocyclic adenine amine of the A2 unit of ORN-X^{Tz} has been functionalized with a 3-chlorobenzyl group. To introduce the *N*6-modified adenosine into ORN-X^{Tz}, a 4-step synthesis pathway was carried out from commercial 6-chloroadenosine to obtain the azide-containing nucleoside **19** (Scheme S2). This starting material was 2',3'-*O*-protected by an isopropylidene group to give **21**. Then, an aromatic electrophilic substitution reaction carried out in basic medium in the presence of 2-chlorobenzylamine enabled functionalization of the adenine base at the *N*6 position of compound **22**. Finally, as before, DPPA followed by sodium azide treatments generated **23** with a 5'-azido function. Finally, after acidic treatment, the nucleoside **19** of interest was obtained (Scheme S2).

In all, over 30 ORN-X conjugates **24-57** were synthesized with different 5'-ends (OH, cap or cap-0) and various linkers between the SAM adenosine mimics and the ORN (Table 1). Substantial quantities (usually in the hundreds of nmoles) of high purity ORN-X were obtained by robust and efficient synthetic methods applied in solid phase: insertion of a modified dinucleoside phosphoramidite during RNA elongation (for ORN-X^{S} and ORN-X^{N} or ORN-X^{Ns}) or post-RNA elongation click chemistry with a CuAAC reaction (for ORN-X^{Tz} and ORN-X^{TzN6}). Both methods are equally effective when the 5' end of ORN-X is OH or Gppp (average yield of 30% and 15%, respectively) but when it comes to ^{7m}Gppp, it would appear that the overall yields of ORN-X^{Tz} synthesis 8.5%) are lower than those obtained by the phosphoramidite route (18.6% average yield). However, the click chemistry is more convenient and rapid for readily obtaining the dinucleoside on solid support than the multi-step preparation of the dinucleoside phosphoramidites.

Table 1
List and data on all synthesized ORN-X conjugates.[a]

5'-end	N°	Sequence 5'—3'	Calc. m/z	Found m/z[b]	Quantities (nmol)[d]
OH	24	X^{S}GUU	1519.10	1518.79	441
	25	X^{S}GUUGU	2170.47	2170.16	241
	26	X^{S}UUA	1503.10	1503.42	261
	27	X^{S}UUAAA	2161.51	2161.01	509

	28	X^{Ns}UAU	1685.23	1685.71	350
	29	X^{Ns}UAUUA	2320.61	2320.57	302
	30	X^{N}UAUUA	2135.45	2135.24	172
	31	X^{Tz}GUU	1555.09	1555.06	343
	32	X^{Tz}GUUGU	2206.47	2206.23	274
	33	X^{Tz}UUA	1538.09	1538.23	291
	34	X^{Tz}UAUUA	2174.47	2174.09	291
Gppp	35	X^{S}GUU	2024.26	2024.65	84
	36	X^{S}GUUGU	2675.64	2675.22	121
	37	X^{S}GUUGU-Cy5	3208.26[c]	3208.61[c]	91
	38	X^{S}UUAAA	2666.68	2667.05	185
	39	X^{N}UAUUA	2641.63	2641.18	184
	40	X^{Tz}GUU	2059.25	2059.44	124
	41	X^{Tz}GUUGU	2710.63	2710.20	162
	42	X^{TzN6}GUU	2183.82	2183.54	140
	43	X^{TzN6}GUUGU	2835.19	2834.98	139
	44	X^{Tz}GUUGU-Cy5	3243.25[c]	3243.76 [c]	31
^{7m}Gppp	45	X^{S}GUU	2039.30	2039.37	153
	46	X^{S}GUUGU	2690.67	2690.84	152
	47	X^{S}GUUGU-Cy5	3222.28[c]	3222.25[c]	46
	48	X^{S}UUA	2022.29	2022.30	251
	49	X^{S}UUAAA	2680.71	2680.70	206
	50	X^{S}UUAAA-Cy5	3213.33[c]	3213.79[c]	65
	51	X^{Ns}UAU	2205.43	2205.24	168
	52	X^{Ns}UAUUA	2840.81	2841.15	193
	53	X^{Tz}GUU	2073.28	2073.11	73
	54	X^{Tz}GUUGU	2724.65	2724.77	47
	55	X^{Tz}UUA	2057.28	2057.04	139
	56	X^{Tz}UUAAA	2715.70	2715.55	105
	57	X^{Tz}UUAAA-Cy5	3248.32[c]	3247.91[c]	62

[a]ORN synthesis scale: 1 µmole
[b]MALDI-TOF characterization in negative mode $[M-H]^-$
[c]MALDI-TOF characterization in negative mode $[M^+-2H]^-$
[d]quantities of isolated compound after IEX-HPLC purification and desalting

2.3. Dose-response testing of ORN-X^S, ORN-X^{Tz}, ORN-X^{Ns} and ORN-X^N conjugates against SARS-CoV-2 nsp16/nsp10 2'-*O*-MTase

To evaluate the possible interaction of ORN-X conjugates with the SARS-CoV-2 2'-*O*-MTase, we tested some of them with the 5'-terminal RNA sequence of SARS-CoV-2 or -CoV to determine their ability to inhibit the 2'-*O*-MTase activity of the nsp16/nsp10 complex. Briefly, purified nsp16 2'-*O*-MTase protein was incubated together with nsp10 protein in the presence of synthetic ^{7m}GpppAC$_4$, radiolabeled ^{3}H-SAM and the ORN-X conjugates. The RNA substrates were next separated from ^{3}H-SAM by diethylaminoethyl (DEAE) filter binding assay (FBA) and the amount of ^{3}H-Met transferred onto the RNA substrates was evaluated by counting the radioactivity associated to filtermat. Dose-response inhibition was performed by pre-incubation of the proteins with increasing concentrations of the best compounds and the IC_{50} values, defined as the inhibitory compound concentration that causes 50% reduction in enzyme activity were determined by Hillslope curve fitting.

The selected conjugates differ in the 5'-extremity (OH, Gppp, ^{7m}Gppp) of the ORN-X and in the dinucleoside (X^S, X^{Tz}, X^{Ns} and X^N) (Table 2). First, when the 5'-end of the conjugates is OH (entries 1-2, 6) or Gppp (entry 3), no inhibition of 2'-*O*-MTase was observed, meaning that ORN-X **26-27**, **33** and **38** are probably not suitable to accommodate the nsp16/nsp10 catalytic pocket. This result is consistent with the capping pathway process in coronaviruses, since 2'-*O*-methylation takes place on an already *N*7-methylated cap. Indeed, conjugates with ^{7m}Gppp and bearing dinucleosides X^S (entries 4-5) or X^{Tz} (entries 7-8) showed submicromolar inhibitory activity irrespective of ORN length, with slightly better inhibition for ORN-X^{Tz} **55-56**. In contrast, conjugates with bulkier, longer Ns and N linkers are much less active in inhibiting 2'-*O*-MTase (entries 9-11). The Ns and N linkers with an ethyl group instead of a methyl group, and thus with an additional methylene, do not seem to be adequate mimics of the 2'-*O*-methylation transition state. Based on this observation, we decided not to use Ns- and N-linked ORN-X conjugates for the remainder of our study and to focus instead on the S- and Tz-linked ORN-X conjugates.

Table 2
IC_{50} values of ORN-X^S, ORN-X^{Tz}, ORN-X^{Ns} and ORN-X^N with SARS-CoV-2 or CoV RNA sequence on nsp16/nsp10 2'-*O*-MTase of SARS-CoV-2

Entry	Linker Series	5'-end	N°	ORN-X sequence[a] 5'—3'	SARS-CoV-2 nsp16/nsp10 IC_{50}[b] (μM)
1	S	OH	26	X^SUUA	n.i[c]
2			27	X^SUUAAA	n.i[c]
3		Gppp	38	X^SUUAAA	n.i[c]
4		^{7m}Gppp	48	X^SUUA	0.580 ± 0.140
5			49	X^SUUAAA	0.511 ± 0.044
6	Tz	OH	33	X^{Tz}UUA	n.i[b]
7		^{7m}Gppp	55	X^{Tz}UUA	0.295 ± 0.020
8			56	X^{Tz}UUAAA	0.172 ± 0.039

9	Ns	^{7m}Gppp	51	X^{Ns}UAU	54.2 ± 26
10			52	X^{Ns}UAUUA	35.6 ± 18
11	N	Gppp	39	X^{N}UAUUA	10.5 ± 2
12	Sinefungin				15 ± 0.59

[a] SARS-CoV-2 5'-terminal RNA sequence: AUUAAA; SARS-CoV 5'-terminal RNA sequence: AUAUUA

[b] concentration inhibiting MTase activity by 50%; mean value from three independent experiments. Dose-response determination by FBA. A) Increasing concentrations of compounds were incubated with 100 nM nsp16 (MTase) and 600 nM nsp10 (Co-factor) of SARS-CoV-2 in the reaction mixture [40 mM Tris-HCl (pH 8.0), 1 mM DTT, 1mM $MgCl_2$, 1.9 μM SAM and 0.1 μM ^{3}H-SAM (Perkin Elmer)] in the presence of 0.7 μM synthetic ^{7m}GpppAC$_4$. Reactions were incubated at 30°C during 60 min and the enzymatic activity was determined by FBA. B) The IC_{50} values were normalized and fitted with Prism (GraphPad) using the following equation: Y=100/(1+((X/IC_{50})^Hillslope)) (n=3; mean value ± SD).

[c] n.i: no inhibition detected at 10 μM of ORN-X conjugate

2.4. Dose-response testing of ORN-X^S and ORN-X^{Tz} conjugates against NS5MTase$_{DV2}$ and NS5MTase$_{ZV}$

In the same way, ORN-X conjugates were evaluated with the dengue and Zika virus 2'-*O*-MTases by measuring the inhibition of the MTase activity of recombinant methyltransferase domain of the non-structural protein NS5 from DV serotype 2 (NS5 MTase$_{DV2}$) and ZIKV. The NS5 MTase$_{DV2}$ and MTase$_{ZV}$ were pre-incubated with increasing concentrations of ORN-X, and the MTase activity was measured by a filter-binding assay (FBA) as previously described. The IC_{50} of some ORN-X^S and ORN-X^{Tz} conjugates were deduced from the Hillslope curve-fitting (**Table 3**).

Table 3

IC_{50} values of ORN-X^S and ORN-X^{Tz} with DENV/ZIKV RNA sequence on NS5 MTases of DV_2 and ZIKV, and on nsp16/nsp10 2'-*O*-MTase of SARS-CoV-2

Entry	Linker Series	5'-end	N°	ORN-X sequence[a] 5'—3'	dengue virus NS5 IC_{50} (μM)[b]	Zika virus NS5 IC_{50} (μM)[b]	SARS-CoV-2 nsp16/nsp10 IC_{50} (μM)[b]
1	S	Gppp	35	X^SGUU	1.18 ± 0.53	n.d[d]	18.70 ± 0.795
2			36	X^SGUUGU	0.152 ± 0.02	0.185 ± 0.019	17.53 ± 2.63
3		^{7m}Gppp	45	X^SGUU	0.882 ± 0.132	n.d	8.50 ± 0
4			46	X^SGUUGU	0.218 ± 0.107	n.d	5.10 ± 0.8
5	Tz	OH	32	X^{Tz}GUUGU	n.i[c]	n.d	n.d
6		Gppp	40	X^{Tz}GUU	0.276 ± 0.045	n.d	n.d
7			41	X^{Tz}GUUGU	0.168 ± 0.055	0.237 ± 0.016	16.20 ± 6.9
8		^{7m}Gppp	53	X^{Tz}GUU	0.344 ± 0.019	n.d	n.d
9			54	X^{Tz}GUUGU	0.196 ± 0.030	n.d	n.d
10	TzN6 Bn	Gppp	42	X^{TzN6}GUU	0.227 ± 0.017	n.d	n.d
11			43	X^{TzN6}GUUGU	0.217 ± 0.080	0.113 ± 0.012	n.d

[a] dengue and Zika viruses 5'-terminal RNA sequence: AGUUGU

[b] concentration inhibiting MTase activity by 50%; mean value from three independent experiments

Dose-response determination by FBA. A) Increasing concentrations of compounds were incubated with 500 nM of NS5 MTase of DV_2 or ZIKV, or 100 nM nsp16 (MTase) and 600 nM nsp10 (Co-factor) of Sars-CoV-2, in the reaction mixture [40 mM Tris-HCl (pH 8.0), 1 mM DTT, 2 μM SAM and 0.1 μM ^{3}H-SAM (Perkin Elmer)] in the presence of 0.7 μM synthetic ^{7m}GpppAC$_4$. Reactions were incubated at 30°C during 30 min and the enzymatic activity was determined by FBA. B) The IC_{50} values were

normalized and fitted with Prism (GraphPad) using the following equation: Y=100/(1+((X/IC_{50})^Hillslope)) (n=3; mean value ± SD)

[c] n.i: no inhibition detected at 10 µM of ORN-X conjugate

[d] not determined

Similarly to the data obtained with nsp16/nsp10 as target, the ORN-X^{Tz} conjugate **32** with a 5'-OH terminus (entry 5, Table 3) did not inhibit $NS5MTase_{DV2}$ confirming that the cap is required for the interplay with both viral 2'-*O*-MTases. On the other hand, whether the conjugates are capped with Gppp or ^{7m}Gppp barely influence the NS5 inhibition efficiency, since it remains in the submicromolar range for most compounds, whatever the S or Tz linker used in the ORN-X conjugate (entries 2 and 4; entries 7 and 9, for instance). This observation is also consistent with the cap methylation process previously described for dengue or Zika viruses, as the same NS5 enzyme catalyses both *N*7- and 2'-*O*-methylation activities and the 2'-*O*-methylation did not depend on the presence of *N*7-methylation of the RNA substrate [11, 12]. Interestingly, ORN-X^{TzN6} **42** and **43** showed IC_{50} values in the same submicromolar range, whereas with introduction of the *N*6-benzyl- modified nucleobase, we expected an increase in inhibitory activity reflecting a better interaction with NS5, as described in the literature [26].

It was previously reported that the 2'-*O*-MTase activity increases with RNA substrate length [59] and we observe here again that 6-nucleotide-long ORN-X^{S} or ORN-X^{Tz} conjugates (**36**, **41**, **46**, **54**) showed more effective inhibitory activity (IC_{50} ≈ 0.2 µM) than the corresponding 4-nucleotide-long ORN-X conjugates (**35**, **40**, **45**, **53**). This significant inhibition seems to anticipate that these 6-mer ORN-X substrates engage a direct interaction with the RNA binding groove of $NS5MTase_{DV2}$. The influence of ORN length is more pronounced on inhibitory activity of ORN-X^{S} (entries 1-2 and 3-4) than on ORN-X^{Tz} (entries 6-7 and 8-9). The difference is negligible between IC_{50} of 4-mer and 6-mer ORN-X^{TzN6} (entries 10-11).

Interestingly, the IC_{50} values against $NS5MTase_{ZV}$ are in the same submicromolar range as those against $NS5MTase_{DV2}$, meaning that the interaction in the RNA binding site would be quite similar as expected regarding the conserved structural organization of both proteins (entries 2, 7, 11). In addition, we assessed substrate sequence specificity by testing some ORN-X with the dengue sequence (**35-36**, **41**, **45-46**) against SARS-CoV-2 nsp16/nsp10 and their inhibitory activity of this 2'-*O*-MTase was 10-fold weaker than against $NS5MTase_{DV2}$, showing that recognition and interaction with NS5 are indeed sequence-specific.

2.5. Protein-compound binding analysis by Fluorescence polarization (FP)

In order to compare the binding properties of the compounds towards the $NS5MTase_{DV2}$, we next determined the affinity constant (K_d) by fluorescence polarization (FP) assay [60, 61]. We thus functionalized at 3'-end with Cy5 the ORN-X conjugates (**37**, **44** and **47**, Table 1) and we first

demonstrated that the addition of the fluorescent dye did not alter the inhibition of the MTase activity of our compounds by filter-binding assay (not shown). Each compound was subsequently incubated with increasing concentrations of NS5MTase$_{DV2}$ protein in the FP assay. The curves show that the protein induced an increase of the FP signal, confirming that NS5MTase$_{DV2}$ interacts with all the three compounds and the deduced apparent K_d values were in the µM range (Table 4**,** Supporting information).

Table 4
Protein-compound binding affinity by fluorescence polarization

Entry	Linker Series	5'-end	N°	ORN-X sequence[a] 5'—3'	dengue virus NS5 K_d (µM)[b]
1	S	Gppp	37	X^SGUUGU-Cy5	1.215 ± 0.225
2		^{7m}Gppp	47	X^SGUUGU-Cy5	1.245 ± 0.035
3	Tz	Gppp	44	X^{Tz}GUUGU-Cy5	1.117 ± 0.084

[a] dengue virus 5'-terminal RNA sequence: AGUUGU
[b] determination of protein-compound binding affinity by fluorescence polarization. A) Increasing concentrations of NS5MTase$_{DV2}$ protein were incubated with the compounds labelled at the 3'-end with Cy5 (**37**, **44** and **47**). B) The dissociation coefficient (K_d) was calculated from the FP data by site-specific binding regression analysis with Hill slope curve fitting using the following equation: Y=Bmax*X^h/(Kd^h + X^h) (Prism GraphPad software).

Given the interesting K_d values, we attempted co-crystallizations, however soaking experiments yielded no results. A meticulous effort in co-crystallization may perhaps provide new structures shedding light on our understanding of the molecular mechanisms governing methylation reactions or MTase inhibitions.

3. Conclusion

In this study, we reported the synthesis of original bisubstrates for the viral 2' *O*-MTases of SARS-CoV-2, dengue and Zika viruses, involving an adenosine as SAM mimic linked to the 2'-OH of the first nucleotide of short (4 or 6 nt) 5'-cap RNA *via* different linkers of various lengths containing *S* or *N* heteroatoms, or a 1,2,3-triazole moiety. We proposed two strategies to synthesize these ORN-X conjugates either by the incorporation of a pre-formed dinucleoside phosphoramidite into the 5'-end of the solid-supported ORN chain, or by click chemistry achieved post-RNA elongation on solid-phase but out of the synthesizer. First, two 3'-phosphoramidite dinucleosides containing *S*- or *N*-linkers were prepared in good yields, following a multi-step synthetic pathway. On the other hand, the 1,2,3-triazole (Tz) linker was readily obtained by a copper-catalyzed alkyne-azide cycloaddition between a 2'-*O*-propargyl adenosine inserted at the 5'-end ORN chain and a 5'-azido adenosine. This approach seems convenient to implement and provides easy access to different conjugates. As the natural substrate of

2'-*O*-MTases is a 5' cap RNA, a cap structure (Gppp or ^{7m}Gppp) was added to the ORN after elongation and before click reaction (in the case of Tz-containing conjugates). The synthetic methods were efficient to afford over hundred nanomoles of each ORN-X conjugate.

Interestingly, some conjugates synthesized with *S* or Tz-linkers have been shown to inhibit the 2'-*O*-MTase nsp16/nsp10 of SARS-CoV-2 or the NS5 of dengue virus with IC_{50} in the submicromolar range, with high selectivity due to the specificity of ORN sequence correlated to each virus. These data suggest a sequence-specific recognition and interaction of ORN conjugates with these viral 2'-*O*-MTases.

Therefore, such ORN-X conjugates can be used for all 2'-*O*-MTases to probe their active site, by adapting the RNA sequence to the RNA substrate of the MTase under investigation. They will be useful tools to obtain structures of MTase / bisubstrate complexes to unravel the cap RNA methylation process. These short ORN inhibitors could be also considered as potential therapeutic agents to interfere with viral MTases involved either in the capping pathway or in 2'-*O*-methylation inner the viral RNA and thus interplay with viral replication. With this aim, further work is now needed to increase the affinity of the inhibitors and modify them to ensure their delivery into the cells and their stability, which is a bottleneck for unmodified oligonucleotides.

4. Experimental section

4.1. Materials and methods

CH_3CN, pyridine, DIEA were distilled from calcium hydride. All dry solvents and reagents were purchased from commercial suppliers (Acros, Alfa Aesar, Sigma Aldrich, TCI Chemicals) and were used without further purification. Thin-layer chromatography (TLC) analyses were carried out on silica plate 60 F_{254}. Purifications by column chromatography were performed using Biotage Isolera 1 system with Flash-Pure Cartridges from Buchi.

^{1}H NMR and ^{13}C NMR spectra were recorded with proton decoupling at ambient temperature on the following spectrometers: Bruker Avance III (400, 500 or 600 MHz). Chemical shifts (δ) are quoted in parts per million (ppm) referenced to the appropriate residual solvent peak: $CDCl_3$ at 7.26 ppm and DMSO-d_6 at 2.50 ppm relative to TMS. 2D NMR experiments including COSY, HSQC and HMBC were achieved to confirm proton assignments. Coupling constants (*J*) are given in Hertz (Hz). Multiplicity are indicated by: s (singlet), d (doublet), t (triplet), q (quadruplet), m (multiplet), br (broad), dd (doublet of doublet). HRMS analyses were obtained with electrospray ionization on a Q-TOF Micromass spectrometer or with a Waters Synapt G25 (Waters, SN: UEB205) spectrometer equipped with positive electrospray source ionization (ESI). The capillary voltage was set to 2 kV and the sampling cone voltage was set to 30 V.

Analytical and semi-preparative high-performance anion-exchange chromatographies were performed on a Thermoscientific Ultimate 3000 system equipped with a LPG3400RS pump or HPG3200BX pump, a DAD 3000 detector and a WPS-3000TBRS autosampler, column oven TCC-3000SD. IEX-HPLC was performed on DNAPac PA200 columns (4x250 mm, 9x250 mm, Thermo Scientific). The following HPLC solvent systems were used: 5% CH_3CN in 25 mM Tris-HCl buffer pH 8 (eluent A) and 5%

CH_3CN containing 400 mM of $NaClO_4$ in 25 mM Tris-HCl buffer pH 8 (eluent B). Flow rates were 1 mL/min, 4 mL/min for analytical, semi-preparative purposes, respectively. UV detection was performed at 260 nm. Chromeleon software was used.
MALDI-TOF mass spectra were recorded on an AXIMA Assurance (Shimadzu Biotech, UK) equipped with 337 nm nitrogen laser, using a saturated solution of 2,4,6-trihydroxyacetophenone in a solution of acetonitrile/ammonium citrate (0.1 M) (1:1; v/v). The samples were mixed with the matrix in a 1:1 ratio (v/v) crystalized on 384-well stainless steel plate and analyzed. UV quantification of ORN-X was performed on a UV-1600 PC UV/visible spectrophotometer (VWR) by measuring absorbance at 260 nm and using quartz cuvettes.

4.2. Chemical syntheses

*4.2.1. Synthesis of dinucleoside phosphoramidite X^S **1***

*S-(3',5'-O-(tetraisopropyldisiloxane-1,3-diyl)-2'-O-methyladenosyl)-5'-thio-2',3'-O-acetyl-adenosine **4***
To a solution of *S*-(3',5'-*O*-(tetra*iso*propyldisiloxane-1,3-diyl)-2'-*O*-methyladenosyl)-5'-thioadenosine **3** (1.6 g, 1.99 mmol, 1.00 eq) in anhydrous pyridine (7.3 mL) was added acetic anhydride (560 µL, 5.57 mmol, 2.8 eq). The reaction mixture was stirred at 0°C for 3 h under argon. Then, solvent was removed under vacuum and the resulting residue was coevaporated three times with toluene (3 x 20 mL) to give **4** as a white solid (1.73 g, 1.95 mmol, 98%). R_f = 0.23 (MeOH/DCM 5:95). ^{1}H NMR (600 MHz, $CDCl_3$) δ 8.35 (s, 1H), 8.26 (s, 1H), 8.08 (s, 1H), 7.99 (s, 1H), 6.18 (br s, 4H), 6.15 (d, *J* = 5.9 Hz, 1H), 6.02 (s, 1H), 5.99 (t, *J* = 5.8 Hz, 1H), 5.63 (dd, *J* = 5.6, 4.0 Hz, 1H), 5.15 (d, *J* = 11.6 Hz, 1H), 5.01 (d, *J* = 11.6 Hz, 1H), 4.74 (dd, *J* = 9.3, 4.7 Hz, 1H), 4.64 (d, *J* = 4.7 Hz, 1H), 4.50 (ddd, *J* = 6.3, 5.1, 4.0 Hz, 1H), 4.23 (dd, *J* = 13.3, 1.7 Hz, 1H), 4.12 (dt, *J* = 9.4, 2.2 Hz, 1H), 4.01 (dd, *J* = 13.4, 2.6 Hz, 1H), 3.23 (dd, *J* = 14.1, 5.1 Hz, 1H), 3.17 (dd, *J* = 14.1, 6.3 Hz, 1H), 2.13 (s, 3H), 2.06 (s, 3H), 1.13 – 0.90 (m, 28H). ^{13}C NMR (150 MHz, $CDCl_3$) δ 169.8, 169.5, 155.9, 155.7, 153.6, 153.1, 150.0, 149.2, 139.0, 138.6, 120.4, 120.3, 88.7, 86.1, 82.5, 81.7, 78.2, 73.8, 73.2, 73.0, 69.6, 59.9, 32.5, 20.8, 20.6, 17.6 – 12.8. HRMS (ESI+): m/z calcd for $C_{37}H_{57}N_{10}O_{10}SSi_2$ $[M + H]^+$: 889.3513, found: 889.3540.

*S-(3',5'-O-(tetraisopropyldisiloxane-1,3-diyl)-2'-O-methyl-N6-phenoxyacetyladenosyl)-5'-thio-N6-phenoxyacetyl-2',3'-O-acetyladenosine **5***
To a solution of **4** (1.16 g, 1.31 mmol, 1.00 eq) in anhydrous THF (13 mL) was added Pac_2O (1.87 g, 6.53 mmol, 5.00 eq) and pyridine (530 µL, 6.53 mmol, 5.00 eq). The reaction mixture was stirred at room temperature for 15 h under argon. After reaction completion, a saturated aqueous $NaHCO_3$ was added. The aqueous layer was extracted with AcOEt and the combined organic extracts were washed with brine, dried over Na_2SO_4 and concentrated under vacuum. The residue was purified by flash column chromatography (silica gel, linear gradient 0-2% MeOH in DCM) to give **5** as a white foam (1.12 g, 0.97 mmol, 74%). R_f = 0.81 (MeOH/DCM 5:95). ^{1}H NMR (600 MHz, $CDCl_3$) δ 9.41 (br s, 1H), 9.38 (br s, 1H), 8.80 (s, 1H), 8.75 (s, 1H), 8.31 (s, 1H), 8.22 (s, 1H), 7.40 – 7.30 (m, 4H), 7.12 – 6.96 (m, 6H), 6.19 (d, *J* = 5.7 Hz, 1H), 6.06 (s, 1H), 6.03 (t, *J* = 5.7 Hz, 1H), 5.65 (t, *J* = 5.0 Hz, 1H), 5.13 (d, *J* = 11.6 Hz, 1H), 5.01 (d, *J* = 11.6 Hz, 1H), 4.92 – 4.80 (m, 4H), 4.75 (dd, *J* = 9.4, 4.7 Hz, 1H), 4.68 (d, *J* = 4.5 Hz, 1H), 4.52 (dt, *J* = 6.8, 4.3 Hz, 1H), 4.23 (d, *J* = 13.3 Hz, 1H), 4.14 (dt, *J* = 9.2, 2.0 Hz, 1H), 4.02 (dd, *J* = 13.5, 2.5 Hz, 1H), 3.26 (dd, *J* = 14.3, 4.5 Hz, 1H), 3.14 (dd, *J* = 14.2, 6.7 Hz, 1H), 2.14 (s, 3H), 2.07 (s, 3H), 1.15 – 0.90 (m, 28H). ^{13}C NMR (150 MHz, $CDCl_3$) δ 169.7, 169.3, 166.6 (2C), 157.0, 157.0, 152.9, 152.6, 151.6, 150.9, 148.6, 148.3, 142.0, 141.6, 129.9, 123.4, 123.3, 122.5, 122.5, 115.0, 115.0, 88.7, 86.4, 82.6, 81.7, 77.9,

73.8, 73.0, 72.7, 69.5, 68.2, 68.1, 59.6, 32.5, 20.6, 20.4, 17.4 - 12.6. HRMS (ESI+): m/z calcd for $C_{53}H_{69}N_{10}O_{14}SSi_2$ $[M + H]^+$: 1157.4248, found: 1157.4249.

S-(2'-O-methyl-N^6-phenoxyacetyladenosyl)-5'-thio-N^6-phenoxyacetyl-2',3'-O-acetyladenosine ***6***

To a solution of **5** (1.12 g, 0.97 mmol, 1.00 eq) in anhydrous THF (9.7 mL) was added $Et_3N.3HF$ (950 µL, 5.81 mmol, 6.00 eq). The reaction mixture was stirred at 40°C for 17 h under argon. After reaction completion, TEAAc buffer 50 mM, pH 7 was added (5 mL). The aqueous layer was extracted with DCM and the combined organic extracts were washed with brine, dried over Na_2SO_4 and concentrated under vacuum. The residue was purified by flash column chromatography (silica gel, linear gradient 0-5% MeOH in DCM) to give **6** as a white foam (710 mg, 0.78 mmol, 80%). R_f = 0.34 (MeOH/DCM 5:95). ^{1}H NMR (600 MHz, $CDCl_3$) δ 9.58 (br s, 1H), 9.56 (br s, 1H), 8.79 (s, 1H), 8.74 (s, 1H), 8.27 (s, 1H), 8.23 (s, 1H), 7.38 – 7.29 (m, 4H), 7.08 – 7.00 (m, 6H), 6.21 (d, *J* = 6.2 Hz, 1H), 6.15 (t, *J* = 5.9 Hz, 1H), 5.91 – 5.80 (m, 2H), 5.65 (dd, *J* = 5.6, 3.6 Hz, 1H), 4.94 – 4.85 (m, 4H), 4.83 (dd, *J* = 7.6, 4.5 Hz, 1H), 4.59 (d, *J* = 11.9 Hz, 1H), 4.57 – 4.50 (m, 2H), 4.34 – 4.24 (m, 2H), 3.94 (dt, *J* = 13.1, 1.8 Hz, 1H), 3.77 – 3.71 (m, 1H), 3.34 (d, *J* = 2.3 Hz, 1H), 3.10 – 2.97 (m, 2H), 2.16 (s, 3H), 2.06 (s, 3H). ^{13}C NMR (150 MHz, $CDCl_3$) δ 170.0, 169.8, 167.0 (2C), 157.2 (2C), 153.0, 152.1, 151.9, 150.8, 149.3, 148.8, 144.1, 142.8, 130.0, 124.3, 123.5, 122.6, 122.6, 115.1, 115.1, 89.1, 88.3, 86.4, 83.2, 81.4, 76.0, 72.7, 72.6, 71.0, 68.4, 68.3, 63.3, 35.0, 20.8, 20.5. HRMS (ESI+): m/z calcd for $C_{41}H_{43}N_{10}O_{13}S$ $[M + H]^+$: 915.2726, found: 915.2732.

S-(5'-O-(4,4'-dimethoxytrityl)-2'-O-methyl-N^6-phenoxyacetyladenosyl)-5'-thio-N^6-phenoxyacetyl-2',3'-O-acetyladenosine ***7***

After three coevaporations of **6** with anhydrous pyridine (40 mL), a solution of **6** (715 mg, 0.78 mmol, 1.00 eq) in anhydrous pyridine (6.0 mL) was heated at 60°C under argon. Then, 4,4'-dimethoxytrityl chloride (449 mg, 1.33 mmol, 1.70 eq) was added in small portions over 30 min. The mixture was stirred for 4 h at 60°C. After cooling to room temperature, a saturated aqueous $NaHCO_3$ was added. The aqueous layer was extracted with DCM and the combined organic extracts were washed with brine, dried over Na_2SO_4 and concentrated under vacuum. The residue was purified by flash column chromatography (silica gel, linear gradient 0-2% MeOH in DCM, 1% pyridine) to give **7** as a beige foam (890 mg, 0.73 mmol, 94%). R_f = 0.35 (MeOH/DCM 2:98). ^{1}H NMR (600 MHz, $CDCl_3$) δ 9.45 (br s, 1H), 9.44 (br s, 1H), 8.78 (s, 1H), 8.68 (s, 1H), 8.63 – 8.58 (m, 3H), 8.25 (s, 1H), 8.21 (s, 1H), 7.70 – 7.64 (m, 1H), 7.46 – 7.39 (m, 2H), 7.37 – 7.17 (m, 7H), 7.09 – 7.00 (m, 6H), 6.83 – 6.76 (m, 4H), 6.16 (d, *J* = 5.9 Hz, 1H), 6.13 (d, *J* = 4.6 Hz, 1H), 6.03 (t, *J* = 5.8 Hz, 1H), 5.59 (dd, *J* = 5.7, 4.0 Hz, 1H), 4.94 – 4.79 (m, 7H), 4.51 (t, *J* = 4.9 Hz, 1H), 4.35 (dt, *J* = 7.0, 4.3 Hz, 1H), 4.21 (q, *J* = 4.1 Hz, 1H), 3.76 (s, 6H), 3.51 (dd, *J* = 10.7, 3.3 Hz, 1H), 3.39 (dd, *J* = 10.8, 4.1 Hz, 1H), 3.15 (br s, 1H), 3.08 (dd, *J* = 14.5, 4.3 Hz, 1H), 3.02 (dd, *J* = 14.4, 6.7 Hz, 1H), 2.13 (s, 3H), 2.03 (s, 3H). ^{13}C NMR (150 MHz, $CDCl_3$) δ 169.8, 169.5, 166.7 (2C), 158.6, 157.1, 157.0, 152.9, 152.6, 151.6, 151.5, 149.8, 149.8, 148.6, 148.4, 144.5, 142.3, 142.2, 136.0, 135.6, 135.6, 130.1, 129.9, 128.2, 127.9, 127.0, 123.7, 123.3, 123.2, 122.4 (2C), 115.0, 115.0, 113.2, 86.7, 86.7, 86.2, 84.3, 82.8, 75.1, 72.7, 72.6, 69.9, 68.2, 68.1, 63.0, 55.2 (2C), 34.1, 20.6, 20.4. HRMS (ESI+): m/z calcd for $C_{62}H_{61}N_{10}O_{15}S$ $[M + H]^+$: 1217.4033, found: 1217.4052.

S-(5'-O-(4,4'-dimethoxytrityl)-3'-O-(2-cyanoethyl-N,N-diisopropylphosphoramidite)-2'-O-methyl-N6-phenoxyacetyladenosyl)-5'-thio-N6-phenoxyacetyl-2',3'-O-acetyladenosine ***1***

To a solution of **7** (890 mg, 0.73 mmol, 1.00 eq) in anhydrous CH_2Cl_2 (5.2 mL) previously passed through an alumina column were added DIEA (0.2 mL, 0.88 mmol, 1.20 eq) and 2-cyanoethyl *N,N*-di*iso*propylchlorophosphoramidite (0.18 mL, 1.02 mmol, 1.40 eq). The mixture was stirred for 1.5 h at room temperature under argon. After reaction completion, ethyl acetate previously washed with a

saturated aqueous $NaHCO_3$ was added and the reaction mixture was poured into saturated NaCl/$NaHCO_3$ 1/1 v/v). The aqueous layer was extracted with ethyl acetate and organic layers were dried over Na_2SO_4. The solvent was concentrated under reduced pressure. The crude material was purified by silica gel chromatography (80-100% DCM in cyclohexane, 1% pyridine then 0-10% acetone in DCM, 1% pyridine) to give a mixture of 50% of the dinucleoside **1** and 50% of the oxidized dinucleoside **8** as a white foam (880 mg). R_f = 0.83 (Cyclohexane/DCM 30:70). ^{31}P-NMR (121 MHz, CD_3CN) δ 150.0, 149.8 HRMS (ESI+): m/z calcd for $C_{71}H_{78}N_{12}O_{16}PS$ $[M + H]^+$: 1417.5112, found: 1417.5106.

4.2.2. Synthesis of dinucleoside phosphoramidite X^{Ns} ***2***

2',3'-O-acetyl-5'-O-tosyladenosine ***10***

To a solution of 5'-*O*-tosyladenosine **11** (1.0 g, 2.37 mmol, 1.00 eq) in anhydrous pyridine (9 mL) was added acetic anhydride (630 µL, 6.64 mmol, 2.80 eq). The reaction mixture was stirred at room temperature for 18 h under argon. Then, absolute EtOH (9 mL) was added and solvents were removed under vacuum. After coevaporations with toluene (3 x 20 mL), **10** (958 mg, 1.90 mmol, 80%) was obtained as a white solid. R_f = 0.87 (MeOH/DCM 10:90). ^{1}H NMR (400 MHz, DMSO-d_6) δ 8.24 (s, 1H), 8.06 (s, 1H), 7.71 – 7.63 (m, 2H), 7.39 (br s, 2H), 7.34 – 7.25 (m, 2H), 6.15 (d, *J* = 5.3 Hz, 1H), 5.94 (t, *J* = 5.6 Hz, 1H), 5.57 (dd, *J* = 6.0, 4.5 Hz, 1H), 4.51 – 4.27 (m, 3H), 2.36 (s, 3H), 2.09 (s, 3H), 2.01 (s, 3H). ^{13}C NMR (100 MHz, DMSO-d_6) δ 169.3, 169.1, 156.1, 152.7, 148.8, 145.0, 139.8, 131.7, 129.8, 127.5, 119.2, 85.6, 79.2, 71.8, 69.7, 69.2, 21.1, 20.3, 20.1. HRMS (ESI+): m/z calcd for $C_{21}H_{24}N_5O_8S$ $[M + H]^+$: 506.1340, found: 506.1365.

3',5'-O-di-tert-butyldimethylsilyl-2'-O-ethylamino-N-(4-nitrobenzene-sulfonyl)-adenosine ***12***

To a solution of **9** (1.42 g, 2.06 mmol, 1.00 eq) in anhydrous DMF (15 mL) were successively added 4-nitrobenzenesulfonamide (831 mg, 4.12 mmol, 2.00 eq), KI (102 mg, 0.62 mmol, 0.30 eq) and K_2CO_3 (851 mg, 6.17 mmol, 3.00 eq). After stirring at 50 °C for 24 h under argon, the reaction was diluted in AcOEt and water. The aqueous layer was extracted with AcOEt and the combined organic extracts were washed with brine, dried over Na_2SO_4 and concentrated under vacuum. The residue was purified by flash column chromatography (silica gel, linear gradient 0-2% MeOH in DCM) to give **12** as a pale brown solid (986 mg, 1.55 mmol, 75%). R_f = 0.67 (MeOH/DCM 5:95). ^{1}H NMR (400 MHz, $CDCl_3$) δ 8.42 (s, 1H), 8.37 – 8.26 (m, 2H), 8.16 (s, 1H), 8.09 – 7.95 (m, 2H), 6.65 (t, *J* = 5.6 Hz, 1H), 6.01 (d, *J* = 3.7 Hz, 1H), 5.75 (br s, 2H), 4.41 (t, *J* = 5.0 Hz, 1H), 4.17 (dd, *J* = 4.8, 3.7 Hz, 1H), 4.05 (dt, *J* = 5.3, 2.7 Hz, 1H), 3.97 (dd, *J* = 11.6, 3.1 Hz, 1H), 3.83 (ddd, *J* = 10.1, 5.0, 3.5 Hz, 1H), 3.75 (dd, *J* = 11.6, 2.4 Hz, 1H), 3.61 (ddd, *J* = 10.3, 7.6, 3.4 Hz, 1H), 3.37 – 3.11 (m, 2H), 0.91 (s, 9H), 0.88 (s, 9H), 0.14 – -0.01 (m, 12H). ^{13}C NMR (100 MHz, $CDCl_3$) δ 155.6, 153.5, 150.1, 149.2, 146.3, 138.8, 128.4, 124.5, 120.4, 88.0, 85.3, 83.9, 70.1, 69.7, 61.7, 43.6, 26.1, 25.8, 18.6, 18.1, -4.5, -4.6, -5.2, -5.3. HRMS (ESI+): m/z calcd for $C_{30}H_{50}N_7O_8SSi_2$ $[M + H]^+$: 724.2972, found: 724.2980.

N-((3',5'-O-di-tert-butyldimethylsilyl)-2'-O-ethyladenosine)-N-4-nitrobenzenesulfonyl)-5'-deoxy-5'-amino-2',3'-O-acetyladenosine ***13***

To a solution of **12** (986 mg, 1.36 mmol, 1.00 eq) in anhydrous DMF (19 mL) were successively added KI (68 mg, 0.41 mmol, 0.30 eq) and K_2CO_3 (564 mg, 4.09 mmol, 3.00 eq). The reaction mixture was stirred at 55°C under argon. Then, **10** (826 mg, 1.64 mmol, 1.20 eq) was added in small portions over 8 h. After stirring at 55°C for additional 16 h under argon, the reaction was diluted in AcOEt (40 mL). Then, a 10% aqueous citric acid solution was slowly added (40 mL) and the aqueous layer was extracted with AcOEt. The combined organic extracts were washed with a saturated aqueous $NaHCO_3$, with

brine, dried over Na_2SO_4 and concentrated under vacuum. The residue was purified by flash column chromatography (silica gel, linear gradient 0-5% MeOH in DCM) to give **13** as a pale brown foam (806 mg, 0.76 mmol, 56%). R_f = 0.40 (MeOH/DCM 5:95). ^{1}H NMR (400 MHz, $CDCl_3$) δ 8.30 (s, 1H), 8.29 (s, 1H), 8.12 (s, 1H), 8.11 – 8.07 (m, 2H), 7.85 – 7.80 (m, 2H), 7.77 (s, 1H), 5.98 (d, *J* = 3.5 Hz, 1H), 5.95 – 5.77 (m, 6H), 5.64 (t, *J* = 5.6 Hz, 1H), 4.55 – 4.37 (m, 2H), 4.18 (dd, *J* = 4.6, 3.6 Hz, 1H), 4.01 – 3.91 (m, 2H), 3.86 – 3.66 (m, 5H), 3.49 (t, *J* = 5.5 Hz, 2H), 2.13 (s, 3H), 2.08 (s, 3H), 0.91 (s, 9H), 0.87 (s, 9H), 0.15 – 0.01 (m, 12H). ^{13}C NMR (100 MHz, $CDCl_3$) δ 169.7, 169.5, 155.8, 155.6, 153.4, 153.2, 149.9, 149.7, 149.4, 145.5, 139.7, 139.3, 128.5, 124.0, 120.5, 120.2, 87.4, 87.0, 84.8, 83.0, 80.9, 73.1, 71.7, 69.8, 69.5, 61.7, 50.6, 48.3, 26.2, 25.8, 20.7, 20.6, 18.6, 18.2, -4.5, -4.7, -5.2, -5.3. HRMS (ESI+): m/z calcd for $C_{44}H_{65}N_{12}O_{13}SSi_2$ $[M + H]^+$: 1057.4053, found: 1057.4055.

N-((3',5'-O-di-tert-butyldimethylsilyl)-2'-O-ethyl-N^6-phenoxyacetyladenosine)-N-4-nitrobenzenesulfonyl)-5'-deoxy-5'-amino-2',3'-O-acetyl-N^6-phenoxyacetyladenosine ***14***

To a solution of **13** (806 mg, 0.76 mmol, 1.00 eq) in anhydrous THF (7.6 mL) were added pyridine (250 µL, 4.57 mmol, 4.00 eq) and Pac_2O (1.31 g, 3.05 mmol, 6.00 eq). After stirring at room temperature for 24 h under argon, the reaction was diluted in AcOEt (40 mL) and washed with saturated aqueous $NaHCO_3$ (40 mL). The aqueous layer was extracted with AcOEt. The combined organic extracts were washed with brine, dried over Na_2SO_4 and concentrated under vacuum. The residue was purified by flash column chromatography (silica gel, linear gradient 0-5% MeOH in DCM) to give **14** as a white foam (770 mg, 0.58 mmol, 76%). R_f = 0.65 (MeOH/DCM 5:95). ^{1}H NMR (400 MHz, $CDCl_3$) δ 9.55 – 9.39 (m, 2H), 8.76 (s, 1H), 8.74 (s, 1H), 8.37 (s, 1H), 8.19 – 8.12 (m, 2H), 8.09 (s, 1H), 7.92 – 7.84 (m, 2H), 7.39 – 7.32 (m, 4H), 7.09 – 7.01 (m, 6H), 6.04 (d, *J* = 3.2 Hz, 1H), 5.99 (d, *J* = 4.8 Hz, 1H), 5.90 (dd, *J* = 5.9, 4.8 Hz, 1H), 5.59 (t, *J* = 5.6 Hz, 1H), 4.86 (s, 4H), 4.53 – 4.39 (m, 2H), 4.19 (dd, *J* = 4.6, 3.3 Hz, 1H), 4.03 – 3.92 (m, 2H), 3.91 – 3.65 (m, 5H), 3.58 – 3.37 (m, 2H), 2.14 (s, 3H), 2.07 (s, 3H), 0.90 (s, 9H), 0.86 (s, 9H), 0.15 – -0.02 (m, 12H). ^{13}C NMR (100 MHz, $CDCl_3$) δ 169.7, 169.5, 166.8, 166.7, 157.2, 157.1, 152.9, 152.7, 151.4, 151.3, 150.0, 148.9, 148.5, 145.5, 142.6, 142.1, 130.0, 128.5, 124.2, 123.5, 123.2, 122.6, 115.1, 87.5, 87.0, 84.9, 83.0, 81.1, 72.9, 71.6, 69.6, 68.2 (2C), 61.5, 50.5, 48.4, 26.2, 25.8, 20.7, 20.5, 18.6, 18.1, -4.5, -4.7, -5.3 (2C). HRMS (ESI+): m/z calcd for $C_{60}H_{77}N_{12}O_{17}SSi_2$ $[M + H]^+$: 1325.4783, found: 1325.4797.

N-(2'-O-ethyl-N^6-phenoxyacetyladenosine)-N-4-nitrobenzenesulfonyl)-5'-deoxy-5'-amino-2',3'-O-acetyl-N^6-phenoxyacetyladenosine ***15***

To a solution of **14** (770 mg, 0.58 mmol, 1.00 eq) in anhydrous THF (5.8 mL) was added $Et_3N.3HF$ (570 µL, 3.49 mmol, 6.00 eq). The reaction mixture was stirred at 40°C for 24 h under argon. After reaction completion, TEAAc buffer 50 mM, pH 7 was added (5 mL). The aqueous layer was extracted with AcOEt and the combined organic extracts were washed with brine, dried over Na_2SO_4 and concentrated under vacuum. The residue was purified by flash column chromatography (silica gel, linear gradient 0-3% MeOH in DCM) to give **15** as a white foam (451 mg, 0.41 mmol, 71%). R_f = 0.41 (MeOH/DCM 5:95). ^{1}H NMR (400 MHz, $CDCl_3$) δ 9.75 – 9.42 (m, 2H), 8.77 (s, 1H), 8.71 (s, 1H), 8.29 – 8.13 (m, 4H), 7.90 – 7.79 (m, 2H), 7.37 – 7.29 (m, 4H), 7.09 – 6.98 (m, 6H), 6.12 (d, *J* = 5.0 Hz, 1H), 6.00 (t, *J* = 5.5 Hz, 1H), 5.92 (d, *J* = 7.0 Hz, 1H), 5.63 (t, *J* = 5.5 Hz, 1H), 4.88 (s, 4H), 4.74 (dd, *J* = 7.1, 4.6 Hz, 1H), 4.42 (dd, *J* = 4.6, 1.3 Hz, 1H), 4.35 (ddd, *J* = 8.5, 5.2, 3.2 Hz, 1H), 4.30 – 4.25 (m, 1H), 3.95 (dd, *J* = 13.1, 1.9 Hz, 1H), 3.84 – 3.73 (m, 2H), 3.68 – 3.59 (m, 1H), 3.55 – 3.47 (m, 2H), 3.47 – 3.38 (m, 1H), 3.16 – 3.05 (m, 1H), 2.18 (s, 3H), 2.10 (s, 3H). ^{13}C NMR (100 MHz, $CDCl_3$) δ 169.9, 169.6, 167.1, 166.9, 157.0 (2C), 152.7, 152.0, 151.2, 150.6, 150.2, 149.1, 148.8, 143.9, 143.7, 143.2, 129.9, 128.5, 124.3, 124.1, 123.5, 122.5, 115.0,

89.2, 88.0, 87.5, 82.1, 81.8, 72.4, 71.4, 70.6, 68.6, 68.2 (2C), 62.9, 51.5, 49.5, 20.6, 20.4. HRMS (ESI+): m/z calcd for $C_{48}H_{49}N_{12}O_{17}S$ $[M + H]^+$: 1097.3054, found: 1097.3027.

N-(4,4'-O-dimethoxytrityl-2'-O-ethyl-N^6-phenoxyacetyl-adenosine)-N-4-nitrobenzenesulfonyl)-5'-deoxy-5'-amino-2',3'-O-acetyl-N^6-phenoxyacetyladenosine ***16***

After three coevaporations of **15** with anhydrous pyridine (30 mL), a solution of **15** (441 mg, 0.40 mmol, 1.00 eq) in anhydrous pyridine (3.1 mL) was heated at 60°C under argon. Then, 4,4'-dimethoxytrityl chloride (204 mg, 0.60 mmol, 1.50 eq) was added in small portions over 30 min. The mixture was stirred for 4 h at 60°C. After cooling to room temperature, a saturated aqueous $NaHCO_3$ was added. The aqueous layer was extracted with DCM and the combined organic extracts were washed with brine, dried over Na_2SO_4 and concentrated under vacuum. The residue was purified by flash column chromatography (silica gel, linear gradient 0-2% MeOH in DCM, 1% pyridine) to give **16** as a white foam (497 mg, 0.36 mmol, 88%). R_f = 0.67 (MeOH/DCM 5:95). ^{1}H NMR (600 MHz, $CDCl_3$) δ 9.55 – 9.41 (m, 2H), 8.71 (s, 1H), 8.68 (s, 1H), 8.62 (m, 3H), 8.26 (s, 1H), 8.22 – 8.18 (m, 2H), 8.06 (s, 1H), 7.93 – 7.87 (m, 2H), 7.77 – 7.57 (m, 1H), 7.47 – 7.39 (m, 2H), 7.39 – 7.24 (m, 6H), 7.24 – 7.18 (m, 1H), 7.07 – 6.99 (m, 6H), 6.86 – 6.79 (m, 4H), 6.07 (d, *J* = 3.5 Hz, 1H), 6.03 (d, *J* = 4.9 Hz, 1H), 5.98 (t, *J* = 5.4 Hz, 1H), 5.61 (t, *J* = 5.4 Hz, 1H), 4.92 – 4.77 (m, 4H), 4.51 – 4.39 (m, 3H), 4.18 (dt, *J* = 5.6, 3.4 Hz, 1H), 3.94 – 3.84 (m, 2H), 3.77 (m, 7H), 3.63 (dd, *J* = 15.3, 8.6 Hz, 1H), 3.60 – 3.48 (m, 2H), 3.42 (dd, *J* = 10.8, 4.1 Hz, 1H), 3.35 (ddd, *J* = 15.1, 6.4, 4.2 Hz, 1H), 2.14 (s, 3H), 2.05 (s, 3H). ^{13}C NMR (150 MHz, $CDCl_3$) 169.9, 169.5, 166.9, 166.8, 158.8, 157.2 (2C), 152.8, 152.7, 151.4, 151.2, 150.0, 150.0, 148.9, 148.5, 144.6 (2C), 142.9, 142.0, 136.1, 135.7 (2C), 130.2, 130.0, 128.7, 128.3, 128.1, 127.1, 124.4, 123.9, 123.6, 123.4, 122.6 (2C), 115.1 (2C), 113.4, 87.7, 86.9, 84.1, 82.5, 81.9, 72.5, 71.7, 69.9, 68.7, 68.2 (2C), 62.9, 55.4 (2C), 50.9, 49.0, 20.7, 20.5. HRMS (ESI+): m/z calcd for $C_{69}H_{67}N_{12}O_{19}S$ $[M + H]^+$: 1399.4366, found: 1399.4338.

N-(5'-O-(4,4'-dimethoxytrityl)-3'-O-(2-cyanoethyl-N,N-diisopropylphosphoramidite)-2'-O-ethyl-N6-phenoxyacetyladenosine)-4-nitrobenzenesulfonyl)-5'-deoxy-5'-amino-2',3'-O-acetyl-N6-phenoxyacetyl-adenosine ***2***

To a solution of **16** (497 mg, 0.36 mmol, 1.00 eq) in anhydrous CH_2Cl_2 (2.5 mL) previously passed through an alumina column were added DIEA (90 µL, 0.50 mmol, 1.40 eq) and 2-cyanoethyl *N,N*-di*iso*propylchlorophosphoramidite (100 µL, 0.43 mmol, 1.20 eq). The mixture was stirred for 1.5 h at room temperature under argon. After reaction completion, ethyl acetate previously washed with a saturated aqueous $NaHCO_3$ was added and the reaction mixture was poured into saturated NaCl/$NaHCO_3$ 1/1 v/v). The aqueous layer was extracted with ethyl acetate and organic layers were dried over Na_2SO_4. The solvent was concentrated under reduced pressure. The crude material was purified by silica gel chromatography (50-100% DCM in Cyclohexane, 1% pyridine then 0-5% acetone in DCM, 1% pyridine) to give **2** as a pale brown foam (317 mg, 0.20 mmol, 56%). R_f = 0.63 (Cyclohexane/DCM 50:50). ^{31}P-NMR (121 MHz, CD_3CN) δ 149.6, 149.2 HRMS (ESI+): m/z calcd for $C_{78}H_{84}N_{14}O_{20}PS$ $[M + H]^+$: 1599.5445, found: 1599.5415.

4.2.3. Synthesis of N6-m-chlorobenzyl adenosine ***19***

5'-deoxy-5'-N-azido-2',3'-O-isopropylidene-N6-(3-chlorobenzyl)adenosine ***23***

To a solution of **22** (500 mg, 1.16 mmol, 1.00 eq) in 1,4-dioxane under argon were added diphenylphosphoryl azide (500 µL, 2.32 mmol, 2.00 eq) and DBU (520 µL, 3.48 mmol, 3.00 eq). After stirring at 25°C for 3 hours, sodium azide (377 mg, 5.80 mmol, 5.00 eq) and 15-crown-5 (23 µL, 0.12 mmol, 0.10 eq) were added and the mixture was stirred at 100°C for 5 hours. After cooling to room temperature, excess of sodium azide was removed by filtration and the filtrate was concentrated to

dryness. The residue was purified by flash column chromatography (silica gel, linear gradient 0 – 2% MeOH in DCM) as the eluent to give **23** (460 mg, 87%) as a white solid. Rf 0.44 (9:1 AcOEt/MeOH). ^{1}H NMR (600 MHz, $CDCl_3$) δ 8.40 (s, 1H), 7.81 (s, 1H), 7.42 – 7.32 (m, 1H), 7.26 – 7.23 (m, 3H), 6.33 (t, *J* = 6.1 Hz, 1H), 6.09 (d, *J* = 2.3 Hz, 1H), 5.46 (dd, *J* = 6.3, 2.2 Hz, 1H), 5.07 (dd, *J* = 6.4, 3.4 Hz, 1H), 4.98 – 4.69 (m, 2H), 4.38 (ddd, *J* = 6.5, 5.1, 3.4 Hz, 1H), 3.66 – 3.47 (m, 2H), 1.62 (s, 3H), 1.39 (s, 3H). ^{13}C NMR (150 MHz, $CDCl_3$) δ 154.9, 153.5, 148.6, 140.7, 139.6, 134.7, 130.1, 127.8, 127.8, 125.8, 120.6, 114.9, 90.8, 85.9, 84.3, 82.2, 52.5, 43.9, 27.3, 25.5. HRMS (ESI+): m/z calcd for $C_{20}H_{22}ClN_8O_3$ $[M+H]^+$: 457.1498, Found 457.1505.

*5'-deoxy-5'-N-azido-N6-(3-chlorobenzyl)adenosine **19***

23 (278 mg, 0.61 mmol, 1.00 eq) was treated at room temperature with TFA in water (8/2, conc. 0.05 M). After stirring for 3 hours, solvents were removed. The residue was diluted with AcOEt (30 mL) and washed with saturated aqueous $NaHCO_3$ (30 mL). The aqueous layer was extracted with AcOEt (3 x 30 mL) and the combined organic extracts were washed with brine, dried over Na_2SO_4 and concentrated under vacuum. The residue was purified by flash column chromatography (silica gel, linear gradient 0 – 5% MeOH in AcOEt) to give **19** (250 mg, 99%) as a white solid. Rf 0.60 (9:1 AcOEt/MeOH). ^{1}H NMR (600 MHz, DMSO-d_6) δ 8.46 (br. s, 1H), 8.40 (s, 1H), 8.24 (s, 1H), 7.49 – 7.15 (m, 4H), 5.95 (d, *J* = 5.3 Hz, 1H), 5.57 (d, *J* = 5.8 Hz, 1H), 5.37 (d, *J* = 5.1 Hz, 1H), 4.85 – 4.61 (m, 2H, $H_{2'}$), 4.21 (q, *J* = 4.8 Hz, 1H), 4.09 – 3.99 (m, 1H), 3.68 (dd, *J* = 13.2, 7.0 Hz, 1H), 3.56 (dd, *J* = 13.1, 3.7 Hz, 1H). ^{13}C NMR (150 MHz, DMSO-d_6) δ 154.8, 153.1, 149.3, 143.2, 140.6, 133.4, 130.6, 127.4, 127.1, 126.3, 120.1, 88.3, 83.4, 78.2, 71.4, 52.2, 42.9. HRMS (ESI+): m/z calcd for $C_{17}H_{18}ClN_8O_3$ $[M+H]^+$: 417.1190, Found 417.1205.

4.3. Oligonucleotide (ORN-X) syntheses

Oligonucleotides syntheses were performed on LCAA-CPG solid support (Biosearch Technologies) at 1 µmole scale using an automated DNA synthesizer (Applied Biosystems 394) with TWIST^{TM} synthesis columns (Glen Research) and oligonucleotide synthesis reagents from Biosearch Technologies. 2'-*O*-PrOM and 2'-*O*-PivOM ribonucleosides, 2'-*O*-propargyl adenosine phosphoramidites were purchased from ChemGenes (MA, USA). 3'-cyanine 5 CPG was obtained from Biosearch Technologies.

After ORN elongation, different treatments depending of 5'-extremity (OH, Gppp, ^{7m}Gppp) of ORN-X conjugates were applied.

For 5'-OH ORN-X^{S} **24-27**, ORN-X^{N} **28-30**, the solid support was treated with a solution of 1M DBU/CH_3CN (2 mL) for 3 min at room temperature. Then, ORN were cleaved from solid support using a 30% aqueous ammonia solution for 3 h at 40°C. The solvents were evaporated under vacuum (in the presence of 500 µL of *iso*propylamine for ORN sequences containing guanosine) [50]. ORN-X were analyzed and purified by IEX-HPLC, and were characterized by MALDI-TOF MS. ORN-X were desalted using a C_{18} cartridge Sep-Pak® Classic.

For GpppORN-X^{S} **35-38**, GpppORN-X^{N} **39**, ^{7m}GpppORN-X^{S} **45-50**, ^{7m}GpppORN-X^{Ns} **51-52**, the 5'-capping steps with GDP or ^{7m}GDP were performed as described in a previous publication [51]. The deprotection treatment was applied as described for 5'-OH ORN-X using 30% aqueous ammonia solution for GpppORN-X or 7M methanolic ammonia solution for ^{7m}GpppORN-X.

For the synthesis of ORN-X^{Tz} **31-34**, **40-44**, **53-57** the CPG beads (1 µmole) were poured in a sealed microwaves tube and azide **18** (100 mM solution in 1,4-dioxane, 30 µL, 3.00 eq), $CuSO_4$ (40 mM solution in water, 10 µL, 0.40 eq), sodium ascorbate (100 mM solution in water, 20 µL, 2.00 eq) and water (20 µL) (water used for dilution was previously flushed under argon for 5 min) were added under argon. The reaction mixture was heated at 65°C under microwaves for 1 h (400 rpm). Then, solid support was

washed with 1,4-dioxane, a 0.1 M aqueous solution of EDTA, water, MeOH, CH_2Cl_2 and dried under argon. Solid support was treated with a solution of 1M DBU/CH_3CN (2 mL) for 3 min at room temperature and ORN were cleaved from solid support and fully deprotected using a 30% aqueous ammonia solution or a 7M methanolic ammonia solution for 3 h at 40°C. Solvents were evaporated under vacuum (in the presence of 500 µL of *iso*propylamine for ORN containing guanosine). ORN-X^{Tz} were analyzed and purified by preparative IEX-HPLC, and were characterized by MALDI-TOF-MS. ORN-X^{TZ} were desalted using a C_{18} cartridge Sep-Pak® Classic, lyophilized and stored at -20°C.

4.4. MTase filter-binding assay (FBA)

The transfer of tritiated methyl from $^{[3H]}$SAM onto RNA substrate was monitored by filter-binding assay, performed according to the method described previously [62]. The recombinant methyltransferase domain of the non-structural protein NS5 from DV serotype 2 ($NS5MTase_{DV2}$) corresponding to residues 1–296 of NS5 was expressed and purified as described previously [63]. FBA was carried out in reaction mixture [40 mM Tris-HCl (pH 8.0), 1 mM DTT, 2 µM SAM and 0.1 µM 3H-SAM (Perkin Elmer)] in the presence of 0.7 µM synthetic $^{7m}GpppAC_4$ and $NS5MTaseDV_2$ protein (500 nM). The enzyme was first mixed with the compound suspended in water before the addition of RNA substrate and SAM and then incubated at 30°C. Reactions mixtures were stopped after 30 min by their 10-fold dilution in ice-cold water. Samples were transferred to diethylaminoethyl (DEAE) filtermat (Perkin Elmer) using a Filtermat Harvester (Packard Instruments). The RNA-retaining mats were washed twice with 10 mM ammonium formate pH 8.0, twice with water and once with ethanol before drying. They were soaked with scintillation fluid (Perkin Elmer), and 3H-methyl transfer to the RNA substrates was determined using a Wallac MicroBeta TriLux Liquid Scintillation Counter (Perkin Elmer). For IC_{50} measurements, values were normalized and fitted with Prism (GraphPad software) using the following equation: Y=100/(1+((X/IC50)^Hillslope)). IC_{50} is defined as the inhibitory compound concentration that causes 50% reduction in enzyme activity.

4.5. Fluorescence polarization (FP)

Compounds containing the sequence that corresponds to the 5’ end of dengue virus (DENV) mRNA and 3’-functionalized with cyanine 5 (Cy5) were incubated (at room temperature for 5 min) with increasing concentrations of $NS5MTase_{DV2}$ protein in reaction buffer [Tris-HCl 50 mM (pH 8), NaCl 50 mM, DTT 1 mM]. FP measurements were performed in 384-well black plate using a microplate reader (PHERAstar FS ; BMG Labtech) with an optical module equipped with polarizer and using excitation and emission wavelengths of 590 and 675 nm, respectively. Dissociation constants (K_d) were determined using one site specific binding with Hill slope curve fitting with the following equation: Y=Bmax*X^h/(Kd^h+X^h) (Prism GraphPad software). K_d is defined as the ligand concentration that binds to half the receptor sites at equilibrium.

Declaration of Competing Interest

The authors declare that they have no known competing financial interests or personal relationships that could have appeared to influence the work reported in this paper.

Funding

This work was supported by the Agence Nationale pour la Recherche (ANR) under MetInCoV grant agreement n°ANR-21-CO14-0004-01 and Virage project ANR-20-CE11-0024-02, the European Union's Horizon 2020 Research and Innovation program under grants no. 101005077 (the CARE project) and the Fondation pour la Recherche Médicale [FDT202204014965]. R. A-B. thanks University of Montpellier for financial support of his PhD work and ANR for funding the post-doc fellowship. J.T salaries were supported by ANR MetInCoV.

Appendix A. Supplementary data

Supplementary data to this article can be found online at :

References

[1] A. Decombe, P. El Kazzi, E. Decroly, Interplay of RNA 2'-O-methylations with viral replication, Curr. Opin. Virol. 59 (2023) 101302. https://doi.org/10.1016/j.coviro.2023.101302.
[2] W. McIntyre, R. Netzband, G. Bonenfant, J.M. Biegel, C. Miller, G. Fuchs, E. Henderson, M. Arra, M. Canki, D. Fabris, C.T. Pager, Positive-sense RNA viruses reveal the complexity and dynamics of the cellular and viral epitranscriptomes during infection, Nucleic Acids Res. 46 (2018) 5776-5791. https://doi.org/10.1093/nar/gky029.
[3] R. Netzband, C.T. Pager, Epitranscriptomic marks: Emerging modulators of RNA virus gene expression, Wiley Interdiscip. Rev. RNA 11 (2020) e1576. https://doi.org/10.1002/wrna.1576.
[4] E. Decroly, F. Ferron, J. Lescar, B. Canard, Conventional and unconventional mechanisms for capping viral mRNA, Nat. Rev. Microbiol. 10 (2011) 51-65. https://doi.org/10.1038/nrmicro2675.
[5] R. Züst, L. Cervantes-Barragan, M. Habjan, R. Maier, B.W. Neuman, J. Ziebuhr, K.J. Szretter, S.C. Baker, W. Barchet, M.S. Diamond, S.G. Siddell, B. Ludewig, V. Thiel, Ribose 2'-O-methylation provides a molecular signature for the distinction of self and non-self mRNA dependent on the RNA sensor Mda5, Nature Immunol. 12 (2011) 137-143. https://doi.org/10.1038/ni.1979.
[6] S.C. Devarkar, C. Wang, M.T. Miller, A. Ramanathan, F. Jiang, A.G. Khan, S.S. Patel, J. Marcotrigiano, Structural basis for m7G recognition and 2'-O-methyl discrimination in capped RNAs by the innate immune receptor RIG-I, Proc. Natl. Acad. Sci. U.S.A. 113 (2016) 596-601. https://doi.org/doi:10.1073/pnas.1515152113.
[7] M. Ringeard, V. Marchand, E. Decroly, Y. Motorin, Y. Bennasser, FTSJ3 is an RNA 2'-O-methyltransferase recruited by HIV to avoid innate immune sensing, Nature 565 (2019) 500-504. https://doi.org/10.1038/s41586-018-0841-4.
[8] P. Ramdhan, C. Li, Targeting viral methyltransferases: an approach to antiviral treatment for ssRNA viruses, Viruses 14 (2022). https://doi.org/10.3390/v14020379.
[9] C. Schindewolf, V.D. Menachery, Coronavirus 2'-O-methyltransferase: A promising therapeutic target, Virus Res. 336 (2023) 199211. https://doi.org/10.1016/j.virusres.2023.199211.
[10] B. Coutard, K. Barral, J. Lichière, B. Selisko, B. Martin, W. Aouadi, M.O. Lombardia, F. Debart, J.J. Vasseur, J.C. Guillemot, B. Canard, E. Decroly, Zika virus methyltransferase: structure and functions for drug design perspectives, J. Virol. 91 (2017). https://doi.org/10.1128/jvi.02202-16.
[11] M.-P. Egloff, E. Decroly, H. Malet, B. Selisko, D. Benarroch, F. Ferron, B. Canard, Structural and functional analysis of methylation and 5'-RNA sequence requirements of short capped RNAs by the methyltransferase domain of dengue virus NS5, J. Mol. Biol. 372 (2007) 723-736. https://doi.org/10.1016/j.jmb.2007.07.005.
[12] L. Liu, H. Dong, H. Chen, J. Zhang, H. Ling, Z. Li, P.Y. Shi, H. Li, Flavivirus RNA cap methyltransferase: structure, function, and inhibition, Front. Biol. 5 (2010) 286-303. https://doi.org/10.1007/s11515-010-0660-y.

[13] H. Dong, D. Ray, S. Ren, B. Zhang, F. Puig-Basagoiti, Y. Takagi, C.K. Ho, H. Li, P.Y. Shi, Distinct RNA elements confer specificity to flavivirus RNA cap methylation events, J. Virol. 81 (2007) 4412-4421. https://doi.org./10.1128/jvi.02455-06.
[14] M. Bouvet, C. Debarnot, I. Imbert, B. Selisko, E.J. Snijder, B. Canard, E. Decroly, In vitro reconstitution of SARS-coronavirus mRNA cap methylation, PLoS Pathog. 6 (2010) e1000863. https://doi.org/10.1371/journal.ppat.1000863.
[15] E. Decroly, C. Debarnot, F. Ferron, M. Bouvet, B. Coutard, I. Imbert, L. Gluais, N. Papageorgiou, A. Sharff, G. Bricogne, M. Ortiz-Lombardia, J. Lescar, B. Canard, Crystal structure and functional analysis of the SARS-coronavirus RNA cap 2'-O-methyltransferase nsp10/nsp16 complex, PLoS Pathog. 7 (2011) e1002059. https://doi.org/10.1371/journal.ppat.1002059.
[16] Y. Chen, H. Cai, J. Pan, N. Xiang, P. Tien, T. Ahola, D. Guo, Functional screen reveals SARS coronavirus nonstructural protein nsp14 as a novel cap N7 methyltransferase, Proc. Natl. Acad. Sci. U. S. A. 106 (2009) 3484-3489. https://doi.org./10.1073/pnas.0808790106.
[17] M. Rosas-Lemus, G. Minasov, L. Shuvalova, N.L. Inniss, O. Kiryukhina, J. Brunzelle, K.J.F. Satchell, High-resolution structures of the SARS-CoV-2 2'-O-methyltransferase reveal strategies for structure-based inhibitor design, Sci. Signal. 13 (2020). https://doi.org/10.1126/scisignal.abe1202.
[18] P. Krafcikova, J. Silhan, R. Nencka, E. Boura, Structural analysis of the SARS-CoV-2 methyltransferase complex involved in RNA cap creation bound to sinefungin, Nature Comm. 11 (2020) 3717. https://doi.org./10.1038/s41467-020-17495-9.
[19] J. Kottur, O. Rechkoblit, R. Quintana-Feliciano, D. Sciaky, A.K. Aggarwal, High-resolution structures of the SARS-CoV-2 N7-methyltransferase inform therapeutic development, Nat. Struct. Mol. Biol. 29 (2022) 850-853. https://doi.org./10.1038/s41594-022-00828-1.
[20] N. Imprachim, Y. Yosaatmadja, J.A. Newman, Crystal structures and fragment screening of SARS-CoV-2 NSP14 reveal details of exoribonuclease activation and mRNA capping and provide starting points for antiviral drug development, Nucleic Acids Res. 51 (2023) 475-487. https://doi.or./10.1093/nar/gkac1207.
[21] A.E. Hodel, P.D. Gershon, F.A. Quiocho, Structural basis for sequence-nonspecific recognition of 5'-capped mRNA by a cap-modifying enzyme, Mol. Cell 1 (1998) 443-447. https://doi.org./10.1016/s1097-2765(00)80044-1.
[22] L.J. Yap, D. Luo, K.Y. Chung, S.P. Lim, C. Bodenreider, C. Noble, P.Y. Shi, J. Lescar, Crystal structure of the dengue virus methyltransferase bound to a 5'-capped octameric RNA, PLoS One 5 (2010). 10.1371/journal.pone.0012836.
[23] P. Skvara, D. Chalupska, M. Klima, J. Kozic, J. Silhan, E. Boura, Structural basis for RNA-cap recognition and methylation by the mpox methyltransferase VP39, Antiviral Res. 216 (2023) 105663. https://doi.org./10.1016/j.antiviral.2023.105663.
[24] T. Viswanathan, A. Misra, S.H. Chan, S. Qi, N. Dai, S. Arya, L. Martinez-Sobrido, Y.K. Gupta, A metal ion orients SARS-CoV-2 mRNA to ensure accurate 2'-O methylation of its first nucleotide, Nat. Commun. 12 (2021) 3287. https://doi.org./10.1038/s41467-021-23594-y.
[25] V. Meynier, L. Iannazzo, M. Catala, S. Oerum, E. Braud, C. Atdjian, P. Barraud, M. Fonvielle, C. Tisné, M. Ethève-Quelquejeu, Synthesis of RNA-cofactor conjugates and structural exploration of RNA recognition by an m6A RNA methyltransferase, Nucleic Acids Res. 50 (2022) 5793-5806. https://doi.org/10.1093/nar/gkac354.
[26] S.P. Lim, L.S. Sonntag, C. Noble, S.H. Nilar, R.H. Ng, G. Zou, P. Monaghan, K.Y. Chung, H. Dong, B. Liu, C. Bodenreider, G. Lee, M. Ding, W.L. Chan, G. Wang, Y.L. Jian, A.T. Chao, J. Lescar, Z. Yin, T.R. Vedananda, T.H. Keller, P.Y. Shi, Small molecule inhibitors that selectively block dengue virus methyltransferase, J. Biol. Chem. 286 (2011) 6233-6240. https://doi.org/10.1074/jbc.M110.179184.
[27] M. Brecher, H. Chen, B. Liu, N.K. Banavali, S.A. Jones, J. Zhang, Z. Li, L.D. Kramer, H. Li, Novel broad spectrum inhibitors targeting the flavivirus methyltransferase, PLoS One 10 (2015) e0130062. https://doi.org./10.1371/journal.pone.0130062.
[28] S.P. Lim, D. Wen, T.L. Yap, C.K. Yan, J. Lescar, S.G. Vasudevan, A scintillation proximity assay for dengue virus NS5 2′-*O*-methyltransferase—kinetic and inhibition analyses, Antiviral Res. 80 (2008) 360-369. https://doi.org/10.1016/j.antiviral.2008.08.005.

[29] S. Spizzichino, G. Mattedi, K. Lauder, C. Valle, W. Aouadi, B. Canard, E. Decroly, S.J.F. Kaptein, J. Neyts, C. Graham, Z. Sule, D.J. Barlow, R. Silvestri, D. Castagnolo, Design, Synthesis and Discovery of N,N'-Carbazoyl-aryl-urea Inhibitors of Zika NS5 Methyltransferase and Virus Replication, ChemMedChem 15 (2020) 385-390. https://doi.org./10.1002/cmdc.201900533.
[30] J. Silhan, M. Klima, T. Otava, P. Skvara, D. Chalupska, K. Chalupsky, J. Kozic, R. Nencka, E. Boura, Discovery and structural characterization of monkeypox virus methyltransferase VP39 inhibitors reveal similarities to SARS-CoV-2 nsp14 methyltransferase, Nature Comm. 14 (2023) 2259. https://doi.org./10.1038/s41467-023-38019-1.
[31] R. Ahmed-Belkacem, P. Sutto-Ortiz, E. Decroly, J.J. Vasseur, F. Debart, Synthesis of adenine dinucleosides 2',5'-bridged by sulfur-containing linkers as bisubstrate SAM analogues for viral RNA 2'-O-methyltransferases, Eur. J. Org. Chem. (2019) 6486-6495. https://doi.org/10.1002/ejoc.201901120.
[32] R. Ahmed-Belkacem, F. Debart, J.-J. Vasseur, Bisubstrate strategies to target methyltransferases, Eur. J. Org. Chem. 22 (2022) e202101481. https://doi.org/10.1002/ejoc.202101481.
[33] C. Atdjian, L. Iannazzo, E. Braud, M. Ethève-Quelquejeu, Synthesis of SAM-adenosine conjugates for the study of m6A-RNA methyltransferases, Eur. J. Org. Chem. 2018 (2018) 4411-4425. https://doi.org/10.1002/ejoc.201800798.
[34] S. Oerum, M. Catala, C. Atdjian, F. Brachet, L. Ponchon, P. Barraud, L. Iannazzo, L. Droogmans, E. Braud, M. Ethève-Quelquejeu, C. Tisné, Bisubstrate analogues as structural tools to investigate m(6)A methyltransferase active sites, RNA Biol. 16 (2019) 798-808. https://doi.org/10.1080/15476286.2019.1589360.
[35] C. Atdjian, D. Coelho, L. Iannazzo, M. Ethève-Quelquejeu, E. Braud, Synthesis of triazole-linked SAM-adenosine conjugates: functionalization of adenosine at N-1 or N-6 position without protecting groups, Molecules 25 (2020) 3241. https://doi.org/10.3390/molecules25143241.
[36] D. Coelho, L. Le Corre, K. Bartosik, L. Iannazzo, E. Braud, M. Ethève-Quelquejeu, Synthesis of bisubstrate analogues for RNA methylation studies using two transition-metal-catalyzed reactions, Chem. Eur. J. 29 (2023) e202301134. https://doi.org/10.1002/chem.202301134.
[37] R. Ahmed-Belkacem, P. Sutto-Ortiz, M. Guiraud, B. Canard, J.-J. Vasseur, E. Decroly, F. Debart, Synthesis of adenine dinucleosides SAM analogs as specific inhibitors of SARS-CoV nsp14 RNA cap guanine-N7-methyltransferase, Eur. J. Med. Chem. 201 (2020) 112557. https://doi.org/10.1016/j.ejmech.2020.112557.
[38] C. Chatrin, S.K. Talapatra, B. Canard, F. Kozielski, The structure of the binary methyltransferase-SAH complex from Zika virus reveals a novel conformation for the mechanism of mRNA capping, Oncotarget 9 (2018) 3160-3171. https://doi.org/10.18632/oncotarget.23223.
[39] B.J. Geiss, A.A. Thompson, A.J. Andrews, R.L. Sons, H.H. Gari, S.M. Keenan, O.B. Peersen, Analysis of flavivirus NS5 methyltransferase cap binding, J. Mol. Biol. 385 (2009) 1643-1654. https://doi.org./10.1016/j.jmb.2008.11.058.
[40] A. El Sahili, J. Lescar, Dengue virus non-structural protein 5, Viruses 9 (2017). https://doi.org/10.3390/v9040091.
[41] E. Decroly, I. Imbert, B. Coutard, M. Bouvet, B. Selisko, K. Alvarez, A.E. Gorbalenya, E.J. Snijder, B. Canard, Coronavirus nonstructural protein 16 is a cap-0 binding enzyme possessing (nucleoside-2'O)-methyltransferase activity, J. Virol. 82 (2008) 8071-8084. https://doi.org/10.1128/jvi.00407-08.
[42] G. Añez, D.A. Heisey, E. Volkova, M. Rios, Complete genome sequences of dengue virus type 1 to 4 strains used for the development of CBER/FDA RNA reference reagents and WHO International standard candidates for nucleic acid testing, Genome Announcements 4 (2016) e01583-01515. https://doi.org/doi:10.1128/genomea.01583-15.
[43] M.A. Marra, S.J. Jones, C.R. Astell, R.A. Holt, A. Brooks-Wilson, Y.S. Butterfield, J. Khattra, J.K. Asano, S.A. Barber, S.Y. Chan, A. Cloutier, S.M. Coughlin, D. Freeman, N. Girn, O.L. Griffith, S.R. Leach, M. Mayo, H. McDonald, S.B. Montgomery, P.K. Pandoh, A.S. Petrescu, A.G. Robertson, J.E. Schein, A. Siddiqui, D.E. Smailus, J.M. Stott, G.S. Yang, F. Plummer, A. Andonov, H. Artsob, N. Bastien, K. Bernard, T.F. Booth, D. Bowness, M. Czub, M. Drebot, L. Fernando, R. Flick, M. Garbutt, M. Gray, A. Grolla, S. Jones, H. Feldmann, A. Meyers, A. Kabani, Y. Li, S. Normand, U. Stroher, G.A. Tipples, S. Tyler, R. Vogrig, D. Ward, B. Watson, R.C. Brunham, M. Krajden, M. Petric, D.M. Skowronski, C. Upton, R.L. Roper, The

Genome sequence of the SARS-associated coronavirus, Science 300 (2003) 1399-1404. https://doi.org/10.1126/science.1085953.
[44] F. Wu, S. Zhao, B. Yu, Y.M. Chen, W. Wang, Z.G. Song, Y. Hu, Z.W. Tao, J.H. Tian, Y.Y. Pei, M.L. Yuan, Y.L. Zhang, F.H. Dai, Y. Liu, Q.M. Wang, J.J. Zheng, L. Xu, E.C. Holmes, Y.Z. Zhang, A new coronavirus associated with human respiratory disease in China, Nature 579 (2020) 265-269. https://doi.org/10.1038/s41586-020-2008-3.
[45] M.S. Drenichev, V.E. Oslovsky, L. Sun, A. Tijsma, N.N. Kurochkin, V.I. Tararov, A.O. Chizhov, J. Neyts, C. Pannecouque, P. Leyssen, S.N. Mikhailov, Modification of the length and structure of the linker of N6-benzyladenosine modulates its selective antiviral activity against enterovirus 71, Eur. J. Med. Chem. 111 (2016) 84-94. https://doi.org/10.1016/j.ejmech.2016.01.036.
[46] S. Kusano, T. Sakuraba, S. Hagihara, F. Nagatsugi, Synthesis of 6-amino-2-vinylpurine derivatives for cross-linking and evaluation of the reactivity, Bioorg. Med. Chem. Lett. 22 (2012) 6957-6961. https://doi.org/10.1016/j.bmcl.2012.08.122.
[47] H. Saneyoshi, K. Tamaki, A. Ohkubo, K. Seio, M. Sekine, Synthesis and hybridization properties of 2′-O-(tetrazol-5-yl)ethyl-modified oligonucleotides, Tetrahedron 64 (2008) 4370-4376. https://doi.org/10.1016/j.tet.2008.02.075.
[48] M.H. Lyttle, P.B. Wright, N.D. Sinha, J.D. Bain, A.R. Chamberlin, New nucleoside phosphoramidites and coupling protocols for solid-phase RNA synthesis, J. Org. Chem. 56 (1991) 4608-4615. https://doi.org/10.1021/jo00015a010.
[49] D.E. Mancheno, A.R. Thornton, A.H. Stoll, A. Kong, S.B. Blakey, Copper-catalyzed olefin aminoacetoxylation, Org. Lett. 12 (2010) 4110-4113. https://doi.org/10.1021/ol101702w.
[50] T. Lavergne, J.-R. Bertrand, J.-J. Vasseur, F. Debart, A base-labile group for 2'-OH protection of ribonucleosides: a major challenge for RNA synthesis, Chem. Eur. J. 14 (2008) 9135-9138. https://doi.org/10.1002/chem.200801392.
[51] M. Noël, T. Guez, Y. Thillier, J.J. Vasseur, F. Debart, Access to high-purity 7mG-cap RNA in substantial quantities by a convenient all-chemical solid-phase method, ChemBioChem e202300544 (2023). https://doi.org/10.1002/cbic.202300544.
[52] A. Sarver, N.K. Scheffler, M.D. Shetlar, B.W. Gibson, Analysis of peptides and proteins containing nitrotyrosine by matrix-assisted laser desorption/ionization mass spectrometry, J. Am. Soc. Mass Spectrom. 12 (2001) 439-448. https://doi.org/10.1016/s1044-0305(01)00213-6.
[53] Y. Thillier, E. Decroly, F. Morvan, B. Canard, J.-J. Vasseur, F. Debart, Synthesis of 5'-cap-0 and cap-1 RNAs using solid-phase chemistry coupled with enzymatic methylation by human (guanine-N7)-methyltransferase, RNA 18 (2012) 856-868. https://doi.org/10.1261/rna.030932.111.
[54] F. Himo, T. Lovell, R. Hilgraf, V.V. Rostovtsev, L. Noodleman, K.B. Sharpless, V.V. Fokin, Copper(I)-catalyzed synthesis of azoles. DFT study predicts unprecedented reactivity and intermediates, J. Am. Chem. Soc. 127 (2005) 210-216. https://doi.org/10.1021/ja0471525.
[55] C. Bouillon, A. Meyer, S. Vidal, A. Jochum, Y. Chevolot, J.-P. Cloarec, J.-P. Praly, J.-J. Vasseur, F. Morvan, Microwave assisted “click” chemistry for the synthesis of multiple labeled-carbohydrate oligonucleotides on solid support, J. Org. Chem. 71 (2006) 4700-4702. https://doi.org/10.1021/jo060572n.
[56] J.M. Holstein, D. Stummer, A. Rentmeister, Enzymatic modification of 5'-capped RNA and subsequent labeling by click chemistry, Methods Mol. Biol. 1428 (2016) 45-60. https://doi.org/10.1007/978-1-4939-3625-0_3.
[57] S. Walczak, A. Nowicka, D. Kubacka, K. Fac, P. Wanat, S. Mroczek, J. Kowalska, J. Jemielity, A novel route for preparing 5′ cap mimics and capped RNAs: phosphate-modified cap analogues obtained via click chemistry, Chem. Sci. 8 (2017) 260-267. https://doi.org/10.1039/C6SC02437H.
[58] Glenn S. Van Aller, Alan P. Graves, Patricia A. Elkins, William G. Bonnette, Patrick J. McDevitt, F. Zappacosta, Roland S. Annan, Tony W. Dean, D.-S. Su, Christopher L. Carpenter, Helai P. Mohammad, Ryan G. Kruger, Structure-based design of a novel SMYD3 inhibitor that bridges the SAM-and MEKK2-binding pockets, Structure 24 (2016) 774-781. https://doi.org/10.1016/j.str.2016.03.010.
[59] B. Selisko, F.F. Peyrane, B. Canard, K. Alvarez, E. Decroly, Biochemical characterization of the (nucleoside-2′O)-methyltransferase activity of dengue virus protein NS5 using purified capped RNA

oligonucleotides 7MeGpppACn and GpppACn, J. Gen. Virol. 91 (2010) 112-121. https://doi.org/10.1099/vir.0.015511-0.
[60] M.D. Hall, A. Yasgar, T. Peryea, J.C. Braisted, A. Jadhav, A. Simeonov, N.P. Coussens, Fluorescence polarization assays in high-throughput screening and drug discovery: a review, Methods Appl. Fluoresc. 4 (2016) 022001. https://doi.org/10.1088/2050-6120/4/2/022001.
[61] H.J. Gaus, R. Gupta, A.E. Chappell, M.E. Østergaard, E.E. Swayze, P.P. Seth, Characterization of the interactions of chemically-modified therapeutic nucleic acids with plasma proteins using a fluorescence polarization assay, Nucleic Acids Res. 47 (2019) 1110-1122. https://doi.org/10.1093/nar/gky1260.
[62] G.C. Paesen, A. Collet, C. Sallamand, F. Debart, J.J. Vasseur, B. Canard, E. Decroly, J.M. Grimes, X-ray structure and activities of an essential Mononegavirales L-protein domain, Nat. Commun. 6 (2015) 8749. https://doi.org/10.1038/ncomms9749.
[63] M.P. Egloff, D. Benarroch, B. Selisko, J.L. Romette, B. Canard, An RNA cap (nucleoside-2'-O-)-methyltransferase in the flavivirus RNA polymerase NS5: crystal structure and functional characterization, Embo J. 21 (2002) 2757-2768. https://doi.org/10.1093/emboj/21.11.2757.